國立臺灣大學電機資訊學院生醫電子與資訊學研究所

碩士論文

Graduate Institute of Biomedical Electronics and Bioinformatics
College of Electrical Engineering and Computer Science
National Taiwan University

Master Thesis

利用結構式照明奈米測繪術(SINAP)觀測癌細胞在不同硬度下絲狀偽足的差異

Characteristics of Cancer-Cell Filopodia on Substrates with Different Stiffness Observed by Structured Illumination Nano-Profilometry

劉宥妊

Yu-Ren Liou

指導教授：郭柏齡 博士

Advisor: Po-Ling Kuo, Ph.D.

中華民國 101 年 6 月

June 2012

致謝

這本論文的完成要感謝很多人的協助及意見，最要感謝的莫過於我的指導教授-郭柏齡老師，在實驗的基礎觀念及思考方向給了我很大的啟發，幫助且指引我碩士研究的方向，老師給我們很大的自由度，總是不厭其煩的聽我們的意見，，導正我並且常常給我很有用的建議，突破許多困難；常常看到郭老師和其他老師們在學術研究上的討論、彼此激發想法，也讓我期許自己在往後無論是研究或是工作上，都可以保有如此一般的思考精神。除了實驗之外，郭老師也很關心我們的生活，對於我們在實驗之外的活動也給予鼓勵與支持，讓我在碩士研究生活的兩年之中，除了實驗之外也過的很充實。另外，還有其他郭老師的朋友，李超煌老師、林耿慧老師、宋孔彬老師、郭清齡老師、阮雪芬老師、林峰輝老師、戴子安老師，在我的實驗，無論是實驗方法或是實驗架構上，提供我技術上及想法上莫大的協助；感謝李超煌老師實驗室的于婺學姊和怡君學姊、林耿慧老師實驗室的林文翌學長、林峰輝老師實驗室的建元學長、李百祺老師實驗室的葉佳倫學長、宋孔彬老師實驗室的蘇璟瑋學長及許瑋真學姊、阮雪芬老師實驗室的陳乃寧學姊、戴子安實驗室的陳泱卉同學，沒有這些實驗室的學長姊和同學不厭其煩的幫助我，這本論文就不會完成，也讓我在這兩年裡，體會到和不同領域、不同背景的人合作、討論及互相幫忙的重要性，也非常感激。

當然還要感謝實驗室成員，一起奮鬥的夥伴-大雄，暑假一來到實驗室，是大雄把這個實驗交給我，幫我起了頭，之後無論在實驗上有什麼問題或是想法也都很開心有大雄可以討論，一起為實驗室大大小小的雜事東奔西跑，也一起開發後門附近好吃的美食，一起熬過了這兩年許許多多的困難，很開心有他可以在實驗室陪我講一些無聊好笑的話。再來很謝謝智傑學長和鴻儒學長，在課堂上及實驗上給我很大的幫助，智傑學長是實驗室的馬蓋先，有什麼事情我跟大雄都會立刻向智傑學長求救，很懷念碩一時三個人在實驗室一起想辦法解決問題的好笑樣子，

真的很開心。在我碩一下時，Pinky 的出現簡直是救星，他幫我在實驗室架設了一台 SINAP，在觀察絲狀偽足方面他也提供我很多經驗，真的很慶幸有他的幫忙。大葉跟佩岑的加入讓我們生物組壯大許多，分擔了許多實驗室雜物及工作，而且有佩岑跟 Pinky 在，實驗室都會很熱鬧，也多了許多活動，變得好溫馨。當然不能漏掉實驗室活動股長小田田，幫我們辦了出遊還有許多活動，突然之間變得很精采，平常可以互相吐槽也很好玩。蔣富昇也是我們的戰友，我們一起吃飯聊天，一起討論功課，很開心可以認識這麼特別的朋友。

特別要感謝一直以來都幫我非常多的學姊-李珣，在研究上教給我很多，從念論文、做實驗、分析數據到論文寫作，給過我的幫助不勝枚舉，在生活上也給我很多支持，讓我在台北生活的這兩年多采多姿，解決我許多生活上的大小問題，是我精神上很大的支柱。感謝縱慾團的成員，一起分享研究生活遇到的許多事，一起安排玩樂行程,讓我對生活總是充滿期待。感謝 LS10 社工團、Summer Amigo、格鬥幫的大學、高中同學們，每次不定期的聚會和聊天都會讓我重新充滿能量。最後，也是最重要的，要感謝我的父母及姐姐，在我研究的過程中，無論什麼都很支持我，也隨時準備好溫暖的家讓我可以依靠。

碩士的這兩年，我學到很多很多，關於研究，也關於生活，這一切的成長無論好壞，都將無窮受用在我未來的日子，很慶幸也很感激，我遇到且得到的這一切。

摘要

本論文利用結構式照明奈米繪測術(SINAP)觀察肺癌細胞在不同基材硬度刺激下絲狀偽足的生長與動態變化。

細胞的移動能力在許多生理反應過程中都扮演著重要的角色,例如組織發育、傷口癒合、腫瘤血管新生、過敏反應以及癌症轉移。之前的研究主要是集中在環境中化學信號對於細胞移動能力的影響，但近年來，有越來越多的研究指出，細胞所生存的微環境會給予細胞許多物理性的刺激，如環境硬度被認為可以影響細胞的移動能力。

以往對於細胞移動能力的觀察，是利用長時間追蹤同一顆細胞，並計算出他在一定時間中可以移動的距離做為此細胞的移動能力，但這種記錄方式需要長時間的累積，在實際醫療的應用上並沒有辦法給予即時的資訊，並且在實體內的實行上也有一定的困難。因此我們希望可以利用細胞外觀的特徵來和細胞的移動能力做連結。在本篇論文中，我們將觀察細胞絲狀偽足的生長及動態和基材硬度的關係，有許多研究已經發現絲狀偽足的生長和細胞的移動能力有正相關，並且我們所使用的細胞株 CL1-5 相對於其同種類細胞株 CL1-0 有較高的轉移能力，之前的研究也指出，這種具有高轉移能力的 CL1-5 其絲狀偽足的數目要比其他低轉移能力的細胞株更多，因此我們相信絲狀偽足的生長及動態會受到基材硬度的影響。

實驗中主要是利用李超煌博士所研發的超解析顯微術-結構式照明奈米繪測術(SINAP)觀察絲狀偽足結構。絲狀偽足的直徑大約只有 100-300 奈米，超越一般光學顯微鏡的繞射限制。而經由 SINAP 顯微術所得到的影像，其橫向解析度可以達 140 奈米，而縱像解析度更可以到達 6 奈米，加上搭配廣視野顯微鏡，不需要利用掃描方式取得二維影像，大幅加快了取像速度，且不需要事先對樣品進行螢光染色，非常適合用來長時間觀察絲狀偽足的動態變化。

由於 SINAP 顯微術需搭配正立顯微鏡來進行樣品的成像，因此所觀察之樣品其底下基材必須具有高折射率的特性，然而先前對於基材硬度對細胞影響的實驗所用可調硬度之基材材料大多為水膠，而水膠的折射率和細胞生存環境相近，並沒有辦法在SINAP系統中成像,因此我們實驗的第一步必須要找出一種折射率高，且可以調整其硬度的基材以符合我們實驗的需求。在本實驗中我們所使用的 PVC 具有高折射率，並可藉由加入塑化劑 DINCH 來調整其硬度。實驗結果證實 PVC 可以成功的應用到 SINAP 系統中，而其硬度符合生理環境硬度之範圍，且其生物相容性和傳統常被使用的生物材料差異不大，因此做為本實驗所選用的基材。

觀察絲狀偽足在不同硬度刺激下生長的實驗結果發現，在軟基材上，細胞具有較多且較長的絲狀偽足；而在硬基材上抑制了肌球蛋白(myosin II)的活性同時抑制張力絲(stress fiber)收縮能力，亦可以發現絲狀偽足在數量及長度上都有明顯的增加，模擬了在軟基材上的效果。因此判斷基材硬度可能是藉由影響張力絲的形成，而張力絲和絲狀偽足的形成機制又互相抗拮，進而影響絲狀偽足的生長。另一方面，我們也觀察絲狀偽足在不同硬度下其伸縮速度。實驗結果發現在不同硬度下所記錄的伸縮速度並無不同，可能和取像時間太長有關，之後必須對此做改善。

藉由此實驗的結果,可以了解到基材硬度對於絲狀偽足數量和長度上的影響，進一步研究其調控機制將對於未來在癌症轉移的治療及診斷上能有所幫助。

關鍵字：絲狀偽足、結構式照明奈米繪測術、肺癌細胞、基材硬度

ABSTRACT

In this thesis, we observed the filopodia formation and dynamics of lung cancer cells (CL1-5) on substrates with different stiffness by structured illumination nano-profilometry (SINAP).

Cell migration plays a key role in various physiological and pathological processes, such as tissue development, wound healing, angiogenesis, inflammation, and cancer metastasis. Most of the previous studies focused on the effects of environmental chemical cues on the cell migration. Recently, some studies have reported that the cell migration could also respond to the environmental mechanical stimuli; for example, the substrate stiffness is one of the most important mechanical stimuli.

The traditional method to measure the cell motility is to trace the moving distance of a cell for an accumulated time. This method however should take a long time thus hard to be exerted in *vivo* and in real-time. Therefore, a way to improve is to observe the cell morphology and relate it to the cell motility. Evidences have shown that the formation of filopodia is related to the cell migration. Furthermore, the CL1-5, which has been shown to be the high invasive lung cancer cell line, has more filopodia than CL1-0, which is low invasive lung cancer cell line. In this study, we made the correlation between the formation of filopodia and the substrate stiffness. We speculated

that the substrate stiffness could modulate the filopodia formation and dynamics through the effects on cell adhesions.

The structured illumination nano-profilometry (SINAP), which is developed by Dr. Lee's group, has lateral resolution of 140 nm and depth resolution of 6 nm. This super-resolution microscopy is advanced in the observation of filopodia, whose diameters are only between 100 and 300 nm. Without fluorescence labeling and two-dimensional scanning, the imaging of SINAP is high speed and very suitable for live-cells observation. However, these techniques require culturing cells on materials of refractive index close to that of glass, while most studies regarding the effects of mechanical cues on cellular dynamics were conducted on hydrogel-based substrates.

Here we report the development of culturing substrates of tunable rigidity and refractive index suitable for SINAP studies. Polyvinyl chloride (PVC)-based substrates were mixed with a softener called Di(isononyl) Cyclohexane-1,2-Dicarboxylate (DINCH). The volume ratios of PVC to DINCH were varied from 1:1 to 3:1. The Young's moduli of the resulting substrates ranged from 20 kPa to 60 kPa. Human lung adenocarcinoma cells CL1-5 were cultured on the composite substrates and cell viability was examined using the MTT assay. The results showed that the PVCs were successfully applied to the SINAP system and had high biocompatibility. Thus in this

thesis, the observation of filopodia formation and dynamics were conducted on the PVC substrates.

The results of cells on different stiffness showed that the cells on soft substrates had more filopodial density and length than those on the stiff substrates. Inhibiting the contractility of the stress fibers with blebbistatin treatment increased the density and length of filopodia on stiff substrates, and mimicked the situation of the cells on the soft substrates. Therefore, a possible but indirect mechanism of the effects of the substrate stiffness on filopodia formation might be the formation of the stress fibers, which antagonize to the formation of the filopodia. On the other respects, we also measured the stretching rate of filopodia on different stiffness. The results showed no difference in the protrusion rate and retraction rate between the soft and stiff substrates. This might resulted from the interval times we took between images. Thus in the future, we should shorten the interval time to observe the filopodia with higher stretching speed.

From this study, we can understand the effects of the substrate stiffness on the filopodial density and length. Further studies are needed to determine the underlying mechanism of these effects. With their medical importance, the results would shed new light on the therapy and diagnosis of the cancer disease.

Keywords: Filopodia, SINAP, Lung Cancer Cell, Substrate Stiffness

CONTENTS

LIST OF FIGURES

LIST OF TABLE

Chapter 1 Introduction

1.1 Motivation

Cancer has remained the first rank of the ten leading causes of death for thirty years in Taiwan. Many researchers have devoted their efforts understanding the mechanism and the therapy of the cancer. The most important stage of cancer progression is the metastasis. The beginning of the metastasis is the differentiation of epithelial cells toward a mesenchymal state, which is called the epithelial to mesenchymal transition or EMT. After EMT, the cell morphology becomes fibroblast like [1]. A key part of the metastasis is the migration of both host cells and tumor cells. Darwinian proposes that the emigration of local cancer cells from the primary tumor to the target sites and the formation of metastasis within distinct organs are triggered by cues from the tumor microenvironment. The tumor microenvironment induces the transient changes in the gene expression and increases cell motility, invasion and metastasis [2]. It is also clear that the interaction between the tumor and the host plays an important role during metastatic progression. Furthermore, assembly of actin-based cytoskeleton, including lamellipodia and filopodia, might be related to the motility of the cancer cells.

There are many evidences that the cells can respond to their environments through soluble chemoattractants, physical and structural properties, such as substrate

microtopography and rigidity [3]. In addition to the chemoattractants, more and more studies put attention on the physical properties of the substrate recently. For example, cytoskeleton assembly and cell spreading are very different on the soft matrix and stiff matrix, and the substrate stiffness also regulates the formation and maintenance of tissues [4-8].

For these reasons, we were interested in the effects of the substrate stiffness on filopodial dynamics, one of the features of cell migration. In this study, we cultured lung cancer cells, CL1-5, on substrates with different stiffness, and observed their filopodia with a super-resolution microscopy, SINAP.

1.2 The Important Role of Cell Migration

Cell migration plays an important role in embryonic development, wound healing, inflammation, and cancer metastasis [9]. In the decays, cancer disease has the highest mortality rate and become a common enemy over world. Actually, the tumor itself is not the main cause of the death, but the cancer metastasis is uncontrollable and causes many current therapies ineffective. Therefore, the invasion and cell motility are among the last frontiers in cancer researches [10].

Cancer cells should escapes from the primary tumor in order to initiate the metastasis. They degrade the local extracellular matrix (ECM) and weaken their

linkages with host tissues. For distant spread, cancer cells should migrate through the stroma to intravasate a lymph or vascular channel. As arriving at the metastatic site, cancer cells should extravasate the vascular and migrate to the target tissues [11]. In the above-mentioned process, how cancer cells control their invasion and migration is a key part of metastatic studies.

Cell migration can be constructed by a series of cytoskeleton organization. The actin filament, which is composed of monomer G-actin, is one of the most important structures in cell migration. At the rapidly growing barbed end, the G-actin polymerization rate is faster than the depolymerization rate, while at the slowly growing pointed end, the depolymerization rate is faster than the polymerization rate. Another force generated by the myosin causes the retrograde flow of the actin filament bundle. High activation at the barbed end emerges membrane protrusions; in the opposite, the faster depolymerization and retrograde flow rate retract the cell membrane. This dynamic of the actin filament drives the moving of the cells. In general, the direction of cell movement is correlated with the cell protrusion (Fig. 1-1) [12].

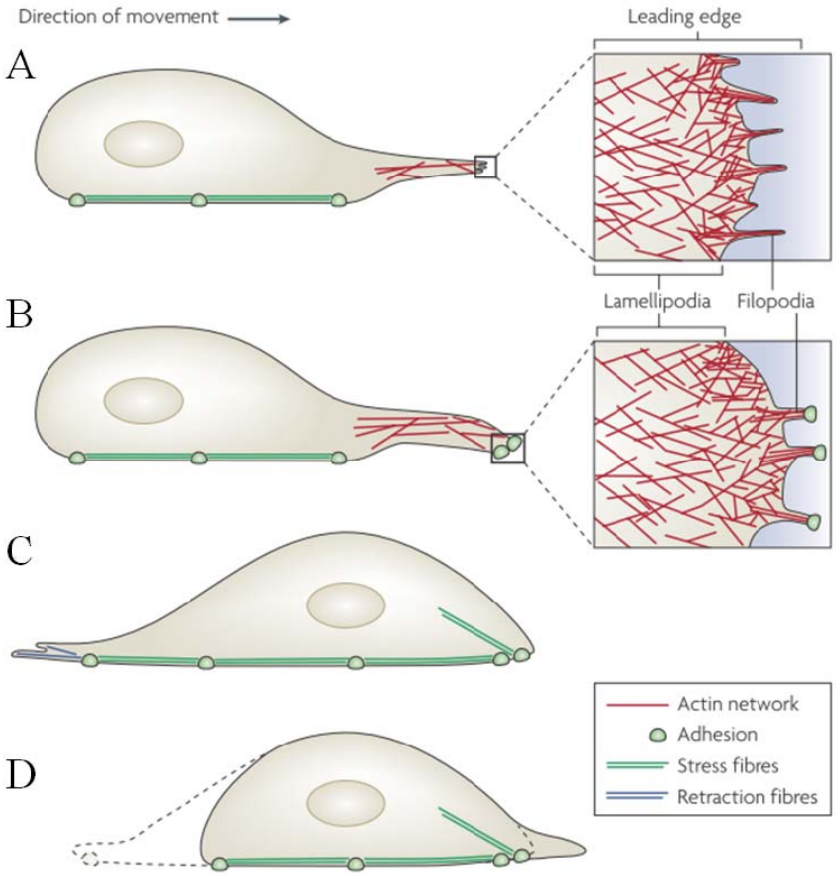

Figure 1-1. Cell migration is dependent on different actin filament structures. [12]

The role of cell motility in cancer metastasis has been highlighted. However, the test of cell motility is tracking a cell for an accumulated time thus hard to be exerted in *vivo* and in real-time. Our way to improve is to observe one of the cell migrating features, the filopodia, which have been shown to relate to the invasive ability of metastatic cancer cells [1]. .

1.3 Introduction of Filopodia

The filopodia are first discovered in 1968 by Vacquier, an American Zoologist [13]. Evidences have shown that filopodia participate in several cellular physiological processes, including cell migration, cell-cell adhesion, and neuronal growth cones, and might be related to the motility of the cancer cells [1, 12].

1.3.1 Structure of Filopodia

Filopodia are one kind of cytoskeleton mainly composed of filamentous F-actin. Different from other actin-based cytoskeletons, lamellipodia and stress fibers, parallel actin filaments in filopodia are cross-linked with the same assembling direction by actin-binding proteins to form tight bundles. At the beginning of filopodia formation, actin filaments are reorganized by the activation of myosin-X, which can promote the convergence of the uncapped or formin-nucleated actin filament barbed ends (the elongating end) into bundles. ENA/VASP proteins can protect actin filaments from capping proteins at the barbed ends, thus continuing the actin elongation and avoiding the branches. The elongating actin filaments are assembled by cross-linking proteins, fascin for example, to generate stiff actin filament bundles. The stiff bundles deform the cell membrane with the help of insulin-receptor substrate p53 (IRSp53) (or other

inverse (I)-BAR domain-containing proteins), facilitate membrane protrusions, and form the filopodia structure (Fig. 1-2) [12].

As the actin filament bundles reach about one-hundred-nm length, myosin-X might navigate barbed-end-directed movement by localizing adhesion proteins to the filopodial tips. The forming of 'tip complex' at the barbed ends, which including Dia2, will gather numbers of actin filament bundles and further elongate the filopodia.

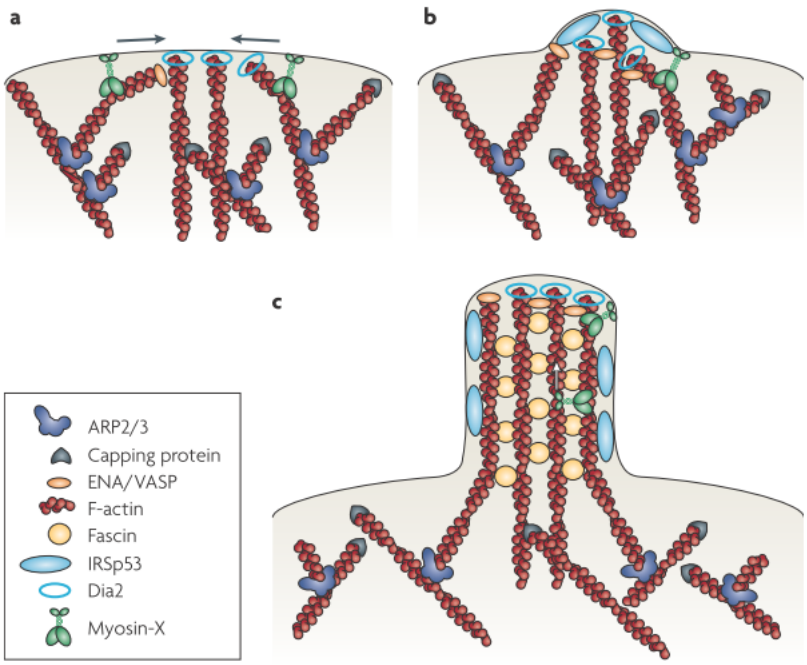

Figure 1-2. A working model for filopodia formation. [12]

1.3.2 The Role of Filopodia in Cell Migration

Studies have shown the correlation between the filopodia and cell motility [9, 11, 14]. It has been investigated that when cells express high levels of cell motility promoting proteins, such as caveolin-1, long form collapsing response mediator

protein-1 (LCRMP-1) or Gb3, the number of filopodia will also increase. Otherwise, when cells express high levels of cell motility inhibiting proteins, collapsing response mediator protein-1 (CRMP-1), the number of filopodia is fewer than cells with lower levels of CRMP-1. Moreover, if filopodia promoting proteins, WAVE or Arp2/3 complex, are inhibited, the number of filopodia decreases and cell motility also declines simultaneously [1]. Overall, cells with higher motility would have more number or more dynamics of filopodia than those with lower motility. Therefore, we could estimate the cell motility or the metastatic ability by observation of the number and the dynamics of the filopodia.

1.3.3 Methods for Filopodia Observation

The diameters of filopodia are within the range between one hundred and three hundred nanometers, which exceed the diffraction limit of the traditional optical microscopy. The high density of actin filaments in filopodia results in relatively higher refractive index than cytoplasm, thus losing the contract under bight-field or phase-contract optical microscopy. In addition to the optical microscopy, scanning electron microscopy can get more detail structural information of filopodia. However, the specimen should be plated a layer of conductive materials and conducted in vacuum

as using the scanning electron microscopy. As the result, scanning electron microscopy could not obtain the live-cell images.

Nowadays, fluorescent labeling is widely used to track a specific target and is applied in most previous studies with filopodia. However, the transfection of fluorescence proteins might alter the nature of the cells. Furthermore, the fluorescence proteins are usually excited by high energy lights, whose phototoxicity might affect the proliferation and activation of the cells and change the dynamic of filopodia [15-16]. Therefore, a super resolution microscopy without fluorescent labeling might be necessary to observe the most natural status of a living cell.

Dr. Chau-Hwang Lee' s group develop a super resolution optical profilometry, called structured-illumination nano-profilometry (SINAP) [17]. The central concept of SINAP is to combine structured-illumination microscopy with differential height images. By projecting a two-dimensional periodic excitation pattern onto the specimen, optical sections are obtained with improved lateral resolution beyond the diffraction limit. Furthermore, as the specimen is placed into the linear region of the optical sectioning axial response curve, the surface profile of the specimen can be calculated by the sharp slope of the linear region. Consequently, both the lateral and the axial resolution of the images can be improved to 140 nm and 6 nm, respectively. SINAP has been successfully used for reconstruction of the three-dimensional morphology of living

cell protrusions [18-19]. In the next chapter, we will introduce the principle of the SINAP system.

1.4 Introduction of Biomechanics

1.4.1 The Cell Motility in Response to Mechanical Stimuli

Cell migration plays a key role in various physiological and pathological processes, such as tissue development, wound healing, angiogenesis, inflammation, and cancer metastasis [9]. It is well known that cell motility can be affected by chemical signals. Recently, more and more studies have indicated that cell movement can also be guided by environmental mechanical stimuli. Since there are wide ranges of stiffness in the body, from soft, neuronal systems with moduli of kilopascal (kPa), to hard, bone tissues with megapascal (MPa), cells show highly dynamic structures and functions in response to different mechanical signals [4-6]. Lo et al. in 2000 first demonstrated that fibroblasts preferentially migrate toward regions of higher stiffness, known as durotaxis [20]. Furthermore, when cells form complex focal adhesion linkages to the substrates, they not only exert force to the substrates but also get feedback from the adhesion sites. As shown in fig. 1-3, cells adhered on stiff substrates receive stronger mechanical feedback, thus leading to more activation of stress-sensitive proteins, stability of focal

adhesions, and the strength of contractile forces. The above process is crucial in sensing system for the cell guidance and may be related to the durataxis. However, different cell types are subject to different stiffness in the body and exhibit different response to matrix rigidity [21]. This is more interesting in cancer metastasis, which is cancer cells migrating from one organ to another and therefore adapting to different environmental stimuli.

1.4.2 Role of Substrate Stiffness in Cancer

The forming of cancer is associated with heterogeneous collections of surrounding cells, including local tissue cells and their extracellular matrix (ECM), various soluble factors, inflammatory cells, and remote target tissues. During tumor initiation and progression, tumor expansion leads to normal tissue disruption, such as tissue compression, interstitial pressure increasing, and tumor stroma abnormal expression, resulting in new elastic moduli of the local environments (Table. 1) [22]. In response to the changing mechanical cues from their environments, cancer cells change their intracellular cytoskeleton organization, actomyosin contraction and cytoskeleton tension [5]. These changes alter the cancer cell morphology, proliferation and motility. For example, studies with human breast cancer reported that highly metastatic and more invasive cancer cells have a reduction in F-actin concentration of as much as 30%,

causing less elastic rigidity than normal cells [23]. Some studies further reported the correlation between the rigidity of the matrix and the organ-specific metastasis [24]. Additionally, stiff substrates stabilize integrin focal adhesion clusters and enhance epithelial growth factor (EGF) signaling, which down-regulates ERK and Rho activity to modulate the cell contractility (Fig. 1-4) [25]. A high level of integrin-ERK-Rho signaling could enhance the cell growth and promote the malignant transformation of a tissue; on the contrary, it would antagonize tumor invasion by stabilizing focal adhesion and inhibiting Rac signaling, which increases cell motility.

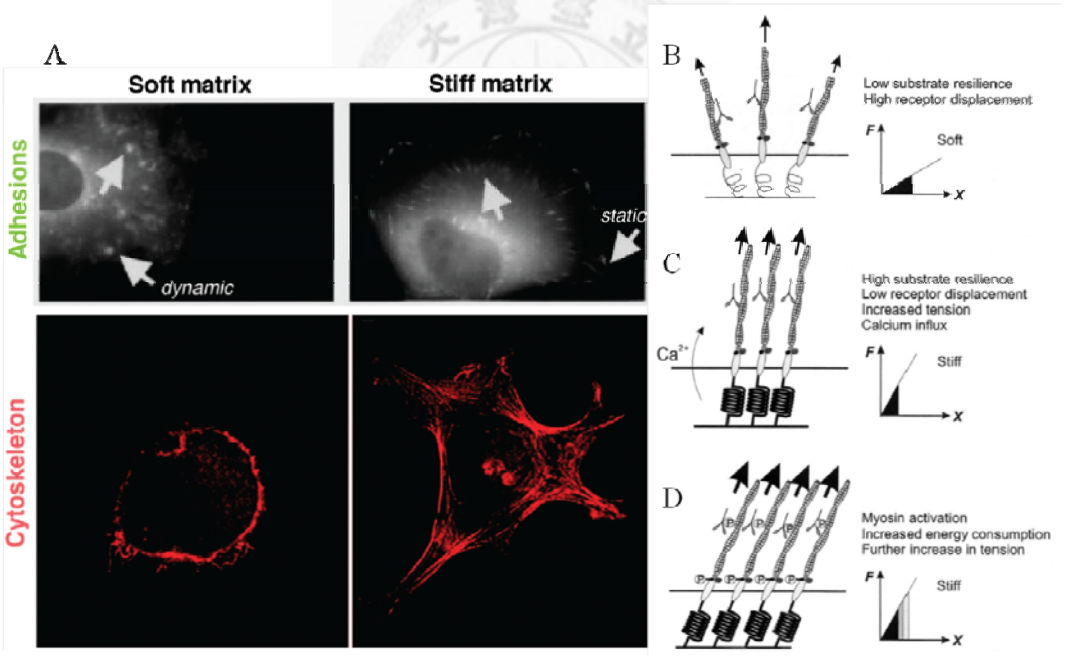

Figure 1-3. (A) The effects of substrate stiffness on adhesion and cytoskeleton organization. On soft substrates, cells show dynamic adhesions (arrow), round cell shape, and unorganized cytoskeleton. On stiff substrate, cells show static focal adhesion, spreading cell shape, and organized stress fibers. (B-D) Model for the detection of matrix rigidity. (B) On the soft substrates, the focal adhesion complex is weak. With a given energy input (*black area* under the force-displacement graph), the complex can move over a long distance (*x* axis). (C) On the stiff substrates, equivalent energy consumption causes a higher tension (*y* axis) and a lower displacement of the complex

(*x* axis). The increase in tension may open the stress-activated channels and induce an influx of extracellular calcium. (D) Calcium then causes the phosphorylation of myosin, thus increasing the energy consumption (*gray area* under the force-displacement graph) and the positive-feedback of tension. [5, 20]

Table 1-1. Elastic moduli of tissues and cells involved in cancer. [22]

		Normal or resting state	Phathological or activated state
Tissue	Breast	0.4-2 kPa	4-12 kPa
	Lung	10 kPa	25-35 kPa
	Brain	0.26-0.49 kPa	7 kPa
	Bone	2-14 Gpa	>689 MPa
	Liver	0.3-0.6 kPa	1.6-20 kPa
Cells	Epithelial cells	~2 kPa	~0.4 kPa
	Fibroblasts	~0.4 kPa	~1 kPa
	Mesenchymal stem cells	0.25-0.9 kPa	N/A
	Macrophages	1.5 kPa	0.5 kPa
	Myeloid	N/A	0.17-1.5 kPa (HL60 cells)
	T lymphocyte	0.013-0.083 kPa (Jurkat cells)	N/A
	Neutrophils	0.07-0.24 kPa	N/A

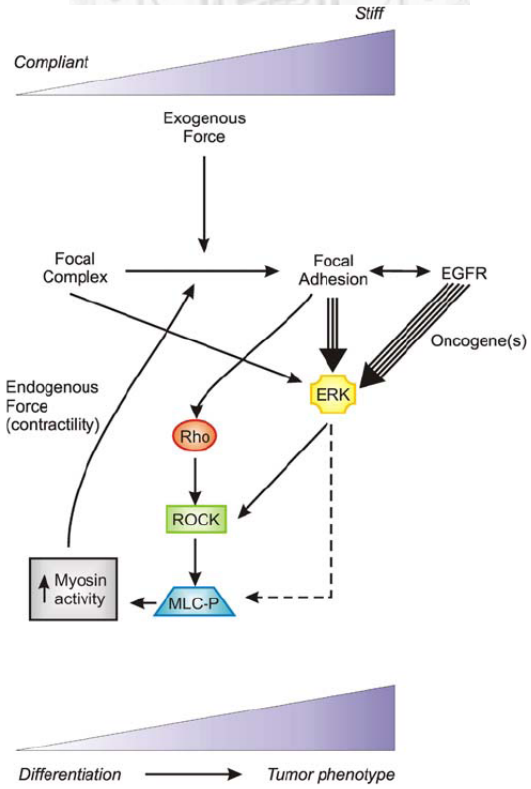

Figure 1-4. Model of tensional homeostasis and force-dependent malignant transformation. [25]

1.4.3 The Effects of substrate stiffness on Filopodia

In the previous section, the mechanical cues from the substrates have been emphasized. Evidences have suggested that matrix rigidity might control the cell morphology, differentiation, and migration. However, the mechanism of the mechanotransduction seems to be still elusive and fragmental. Some studies investigated that cells sense the rigidity by integrin-mediated stretchy [26]. From the ECM to the inside of the cell, the matrix-integrin bonds are the primary links. Integrin is a transmembrane heterodimer composed of an α and a β chain and important in the forming of focal adhesions. A model of the "motor-clutch" force transmission system simulates the traction dynamics of filopodia on compliant substrates with the counterbalance between adhesion clutches and myosin-driven F-actin retrograde flow (fig. 1-5) [27]. The model demonstrates distinct contraction behaviors of filopodia on stiff or soft substrates. Furthermore, the stability of the focal adhesion might be influenced by the substrate stiffness and then down-regulates the activity of Rho-family proteins [25]. Rho-family proteins involve in the dynamics of actin filaments and migration: Cdc42 in filopodia formation and Rho in stress fibers formation, actomyosin assembly and adhesion. High cellular levels of active Rac most often correlate with low levels of active Rho, thus performing strikingly different cell morphology [28]. Studies

with mesenchymal stem cells find that soft substrates inhibit Rho-induced stress fiber formation and α-actin assembly [29].

As the above-mentioned, the filopodial number and dynamics are highly correlated with cell motility. With the Evidences that the soft substrates might inhibit the formation and contractility of the stress fibers, the antagonist of the filopodia formation pathway, we speculated that the soft substrates might therefore enhance the formation of the filopodia. However, because of the limitation of the observation technology, previous studies mostly focus on the changing of cell the migrating direction or cell polarity, which tracking cells for an accumulated times. For understanding how substrate stiffness affects the cancer-cell filopodia, the real-time observation of filopodia activity must be necessary. In this study, we focused on the filopodia activity of lung cancer cells, CL1-5, under different substrate stiffness. To further clarify the underlying mechanism, we speculated that the substrate stiffness could affect the formation of the filopodia through the effects on the cell adhesions. Therefore, we also inhibited the formation and contractility of the stress fibers on stiff substrate by treating with blebbistatin, a myosin II inhibitor, which would then weaken the focal adhesions. The results would make progress in the understanding of the mechanism of cancer metastasis.

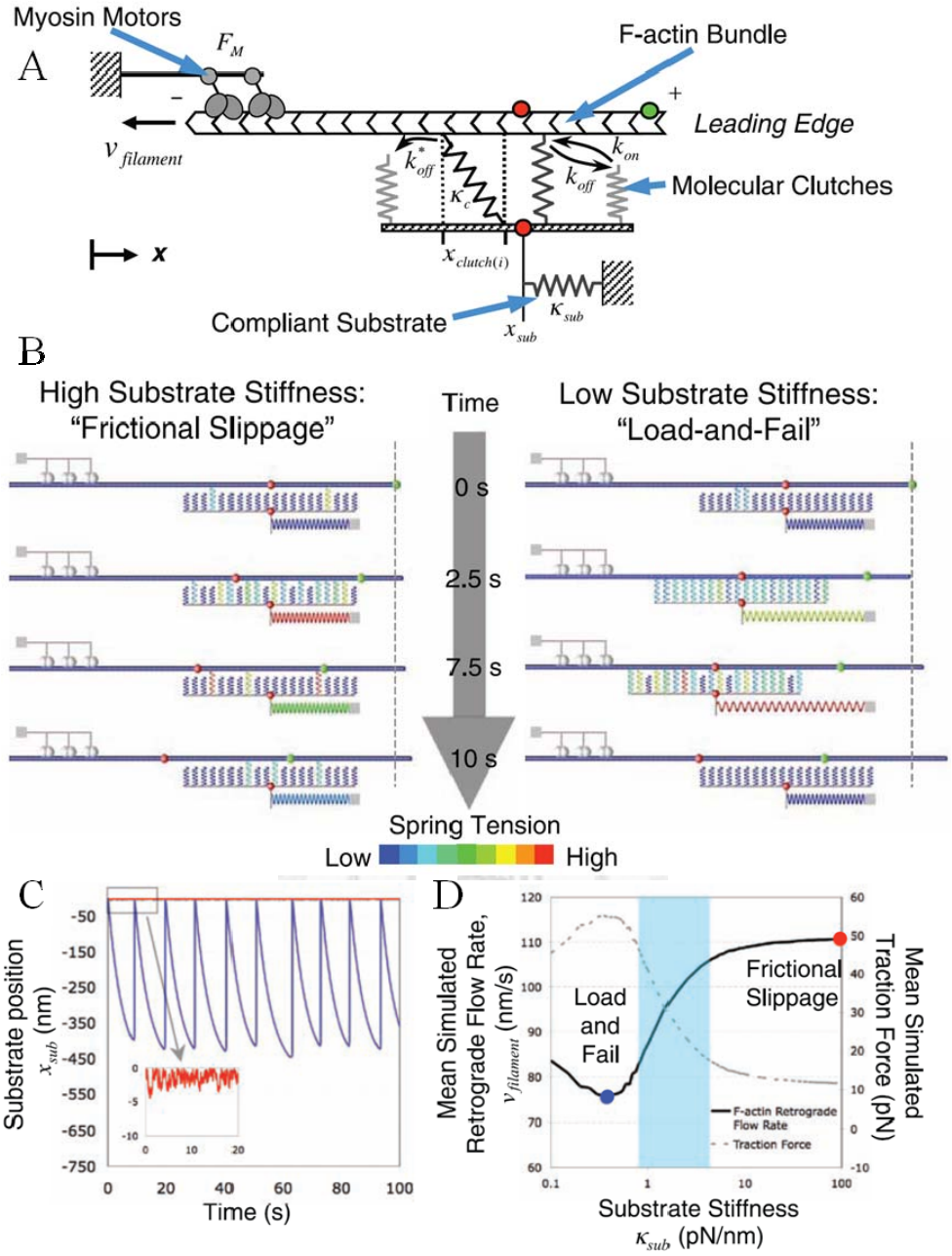

Figure 1-5. A model for motor-clutch motility on compliant substrates predicts substrate stiffness-dependent dynamics. (A) Schematic presentation of a mechano-chemical motor-clutch model. Overall, myosin motors give the actin filament a retrograde flow with force, F_M, at velocity, $v_{filament}$. The mechanical stiffness of the clutches, κ_c, and of the substrate, κ_{sub}, applies resistance force to loading. k_{on} and k_{off} represent the rates of engagement of clutches on F-actin and off F-actin respectively; k_{on}* and k_{off}* are as the clutch is loaded with a force. $x_{clutch}(i)$ represents the strain of stretched clutch. (B) Model of substrate stiffness-dependent clutch dynamics on soft or stiff substrates. (C) Prediction of the substrate position under the loading over time. (D) The simulation of retrograde flow rate on different substrate stiffness. [27]

Chapter 2 Structured Illumination nano-profilometry (SINAP)

In our study, we observed the filpodia of lung cancer cells, which are subject to substrates with different stiffness, by advanced optical techniques, structured-illumination nano-profilometry (SINAP). SINAP combines the concepts of the structured-illumination microscopy and the differential confocal microscopy to enhance the resolution and contract of the images. In this chapter, the principle of the SINAP and the setup will be introduced.

2.1 Differential Confocal Microscopy

Differential confocal microscopy is a realization of differential detection concept [18-19, 30]. Applying the response curve of diffraction effect, differential confocal microscopy has nanometer depth resolution. The depth resolution is limited by the noise from the system and environment, while the lateral resolution is determined by the diffraction limit. Differential confocal microscopy, which gets the images rapidly without optical-axial scanning and provides nanometer axial resolution without contact, is very suitable for live-cell observations.

The setup of differential confocal microscopy is similar to the standard confocal microscopy (Fig2-1)[31]. Photo-detector can detect the strongest signal when the light beam is focused on the sample, reflected or diffracted by the sample, and then mostly passed through the pinhole (which can remove noise from the defocus plane). The detected signals decline as the sample leaves the focal plane. The relation between signal strength and the sample position can be represented as a $\text{sinc}^2(z)$ function with diffraction theory, where z stands for the position of the sample at the optical axial. The peak shows as the sample is located at the focal plane. However, because the slop at the peak is zero, the signal strength is not sensitive to the axial position of the sample. In fact, the depth resolution at the focal plane is about only 0.1 micrometer.

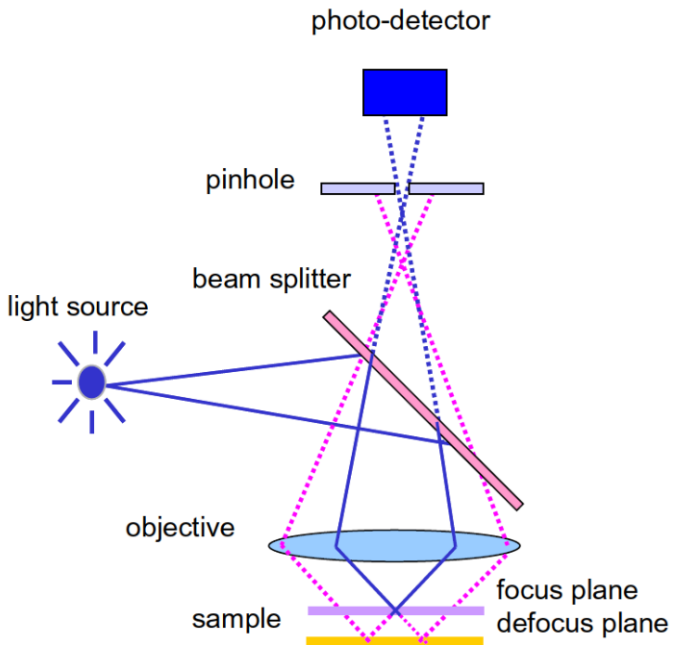

Figure 2-1. The setup and principle of a confocal microscopy. [31]

In contrast, differential confocal microscopy works in the sharp linear region of the optical-sectioning axial response curve of confocal microscopy (fig. 2-2). In this region, the signal strength is highly sensitive to the axial position of the sample. For example, if the slop of the linear region is 1/μm, the 10-nm change in axial position changes the signal strength by 1%, yielding high depth resolution. Additionally, assuming the reflectivity of the sample is known or constant, the topography of sample surface can exactly correspond to different signal strengths. Based on the above benefits, the differential confocal microscopy can provide nanometer depth resolution with structured illumination, and described in next section [32].

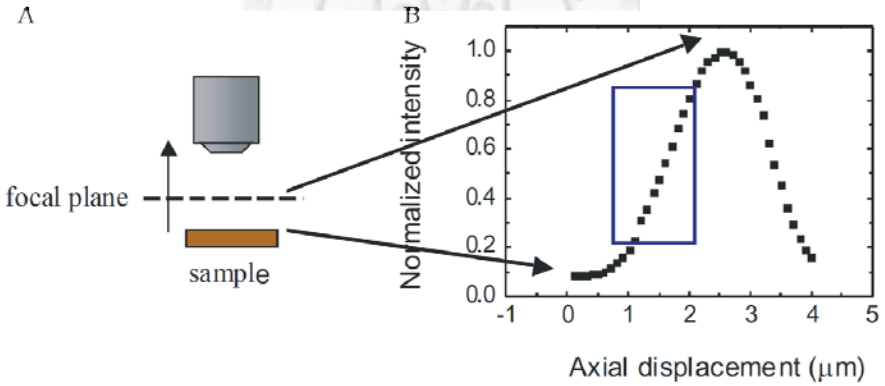

Figure 2-2. (A) Positions of the specimen along optical-sectioning axial correspond to their signal intensity on the response curve. (B) The response curve of the confocal microscopy. The blue square represents the linear region of the response curve. [32]

2.2 Wide-Field Optical Sectioning Microscopy

Wide-field optical sectioning microscopy was first developed by Dr. Tony Wilson's group in 1997 [33]. By projecting a single-spatial-frequency grid pattern onto

the sample, recording three images with the grid pattern at different spatial phases, and using the homodyne detection principle to remove the grid pattern, one can obtain optically sectioned images similar to those obtained by the confocal microscopy [18].

The image is modulated by projecting a single-spatial-frequency grid pattern onto the sample. As the patterns are shifted by 1/3 period, we can record three images with the grid pattern at different spatial phases (Fig. 2-3(b)). Their signal strength can be represented as below:

$I_1=Acos(\theta)$ (2.1)

$I_2=Acos(\theta+2\pi/3)$ (2.2)

$I_3=Acos(\theta+4\pi/3)$ (2.3)

Using the square-law detection principle,

$$I = \sqrt{(I_1 - I_2)^2 + (I_1 - I_3)^2 + (I_2 - I_3)^2} \quad (2.4)$$

, with formula (2.1), (2.2), and (2.3), the grid pattern can be removed to obtain the optically sectioned images, I in the formula (2.4) (Fig. 2-3(b)) [18].

Figure 2-3. (A) Modulated images shifted by 1/3 periodic phase. (B) Reconstructed image with square-law detection principle. [18]

Furthermore, because of the high spatial frequency of the grid, the pattern is clearly imaged only at the focal plane. When the samples are scanned along the optical axial, their signal response curves are similar to those of the confocal microscopy; thus the principle of the differential confocal microscopy can be applied to obtain the depth information (fig. 2-4). In addition, the wide-field optically sectioning microscopy performs real-time three-dimensional imaging without lateral scanning, enhancing the image rate of optically sectioning microscopy.

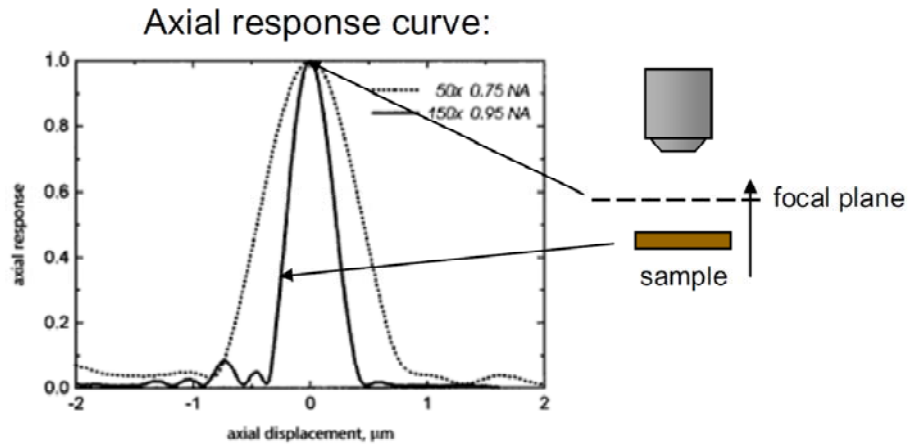

Figure 2-4. The axial response curve of the wide-field optical sectioning microscopy. [18]

2.3 Structured Illumination Microscopy

At the aspect of the Fourier optics, the sample can be expanded by Fourier transform to be a complex grating with different spatial-frequencies. Because of diffraction property, as the light source encounters the grating, it will be deflected out. The higher spatial-frequency the grating has, the bigger the deflection angle is. When the deflection light is out of the objective, the high-frequent signal will be lost, thus

limiting the resolution, which is so called optical diffraction limit. Optical diffraction limit can be calculated as about 0.61λ/NA, or λ/2, where λ is the wavelength of light source and NA is the lens aperture of the objective.

The principle of structured illumination microscopy (SIM) is to add a modulating pattern as the secondary grating to guide the deflected light with high-frequent signals into the objective, thus improving the lateral resolution (fig. 2-5) [34].

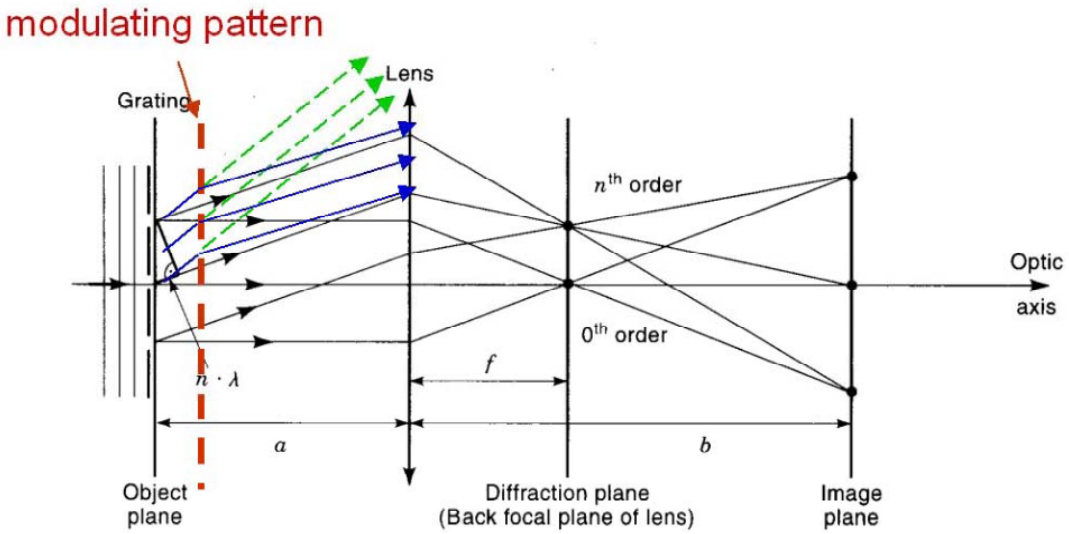

Figure 2-5. The principle of the structured illumination microscopy. [34]

From Fourier transforms of the wide-field optical images, we can get their frequency information or optical transfer function (OTF) (fig. 2-6). Namely, the system will have higher resolution with bigger OTF. For the purpose, a spatially modulated pattern illuminates a specimen and the phase is shifted by 2π/3 every image. The modulated image can be reconstructed by homodyne detection principle (formula 2.5) with three acquired images.

$$I_+ = \frac{1}{3}\left|I_0 + I_1\, exp\left(j\frac{2\pi}{3}\right) + I_2 exp\ \left(j\frac{4\pi}{3}\right)\right| \quad (2.5)$$

From Fourier transforms of the modulated image, it is shown that the center of spatial spectrum shifts to higher frequency (fig. 2-7(B) red arrow) and the OTF obtains the higher spatial-frequency information (fig. 2.7(B) white arrow) [34].

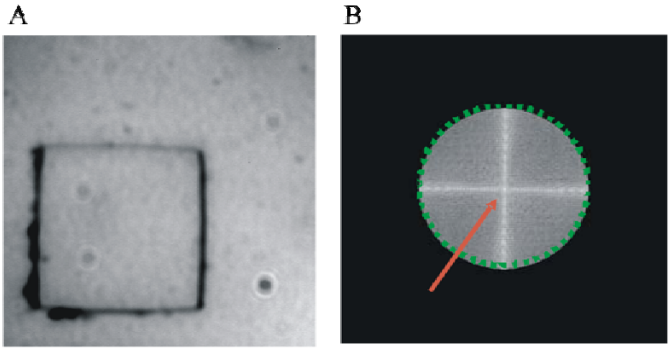

Figure 2-6. (A) A standard wide-field optical image. (B) The spatial spectrum from Fourier transforms of the wide-field optical image. The green dotted circle represents the optical transfer function, and the red arrow indicates the center of spatial spectrum [34]

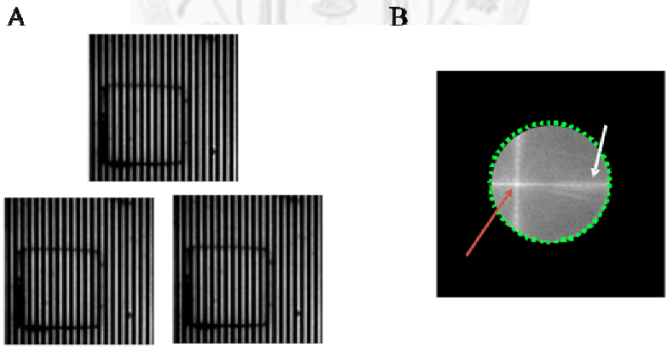

Figure 2-7. (A) Three images with 2π/3-shifted phase. (B) The spatial spectrum and optical transfer function of the reconstructed image by homodyne detection principle. The red arrow represents the original center of spatial spectrum, and the white arrow represents the higher spatial-frequency information after modulation. [34]

To achieve 2-D super-resolution, 2D-mesh illumination instead of 1D grid excitation brings four additional high spatial-frequency components into the imaging system's OTF (fig. 2-8) [34].

$$I_{x\pm}(x,y) = \frac{1}{3}\left|I_0(x,y) + I_1(x,y)exp\left(\mp j\frac{2\pi}{3}\right) + I_2(x,y)exp\left(\pm j\frac{4\pi}{3}\right)\right| \quad (2.6)$$

$$I_{y\pm}(x,y) = \frac{1}{3}\left|I_0(x,y) + I_1(x,y)exp\left(\mp j\frac{2\pi}{3}\right) + I_2(x,y)exp\left(\pm j\frac{4\pi}{3}\right)\right| \quad (2.7)$$

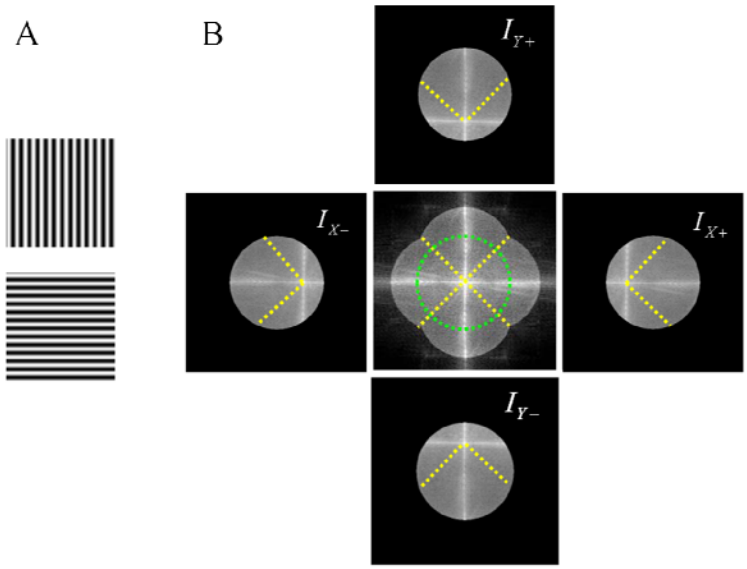

Figure 2-8. (A) Two-dimensional-mash illumination grids. (B) Additional four spectrums with high-frequency information amplify the OTF of the image (central image). Green dotted circle indicates the original OTF, while the reconstructed image obtains larger OTF. [34]

Structured illumination microscopy can enhance spatial resolution and obtain optical section at the same time. Combined with the principle of differential confocal microscopy, which the axial position and signal strength are linear correlation, SIM can be applied to surface topography measurement. The system breaks the diffraction limit to have nanometer spatial resolution and depth resolution at the meanwhile, which is named as structured illumination nano-profilometry, SINAP.

Consequently, with the advanced microscopy, SINAP, both the lateral and the axial resolution of the images can be improved to 140 nm and 6 nm, respectively (fig.

2-9). SINAP has been successfully used to reconstruct the three-dimensional morphology of living cell protrusions [17-19]. This technique however requires culturing cells on substrates with refractive index close to that of glass, while most studies regarding the effects of mechanical cues on cellular dynamics were conducted on hydrogel-based substrates, which possess refractive indices close to that of water [35-37].

In this work, the feasibility of polyvinyl chloride (PVC)-based substrates for SINAP application was investigated.

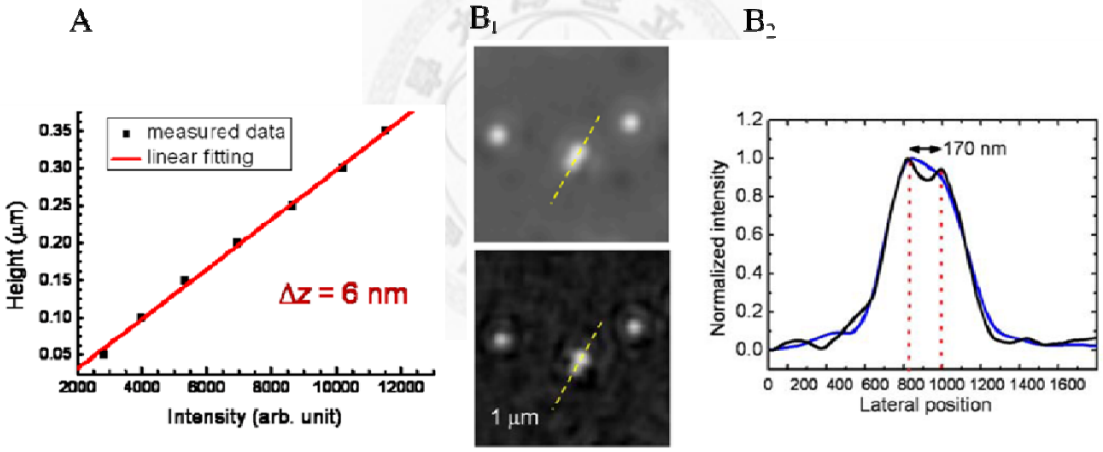

Figure 2-9. (A) The depth resolution of SINAP. (B) The lateral resolution of SINAP. (B_1) Images of an 80-nm-diameter bead. The upper bright field image is compared to the lower SINAP image. (B_2) Comparison of later resolution between the bright field image and the SINAP image. [38]

Chapter 3 Culturing Cells on Flexible Substrates of High Refractive Indexes

Mechanical cues are shown to regulate the cell motility. In this study, we utilized the super-resolution microscopy, SINAP, to study the real-time filopodial activities of lung cancer cells under the stimulations of substrates stiffness. SINAP, as mentioned in previous chapter, should project a high spatial-frequency grating onto the specimen and extract the super-resolution images by collection of reflected signals with periodic phases. This technique however requires the refractive-index difference between the specimen and their underlying substrates, thus reflecting the signals of the samples. Unfortunately, most studies regarding the effects of mechanical cues on cellular dynamics were conducted on hydrogel-based substrates, for example, polyacrylamide (PA) gel, most commonly used, and poly(ethylene glycol) (PEG), whose refractive indices are close to those of the culturing environments. Therefore, these materials are not suitable for SINAP. Here we report the development of cultured substrates with tunable rigidity and suitable refractive index for SINAP applications.

3.1 Introduction of plasticizer-poly(vinyl chloride) (PVC)

Poly(vinyl chloride) (PVC) has been widely used in fields of industrial and biomedical, such as wound-healing suture materials, artificial ligaments and bone fixators, due to its light weight, easy processing, and low cost (fig. 3-1). Additional uses are coating for sensors and pacemakers as well as drug delivery systems within the body [39].

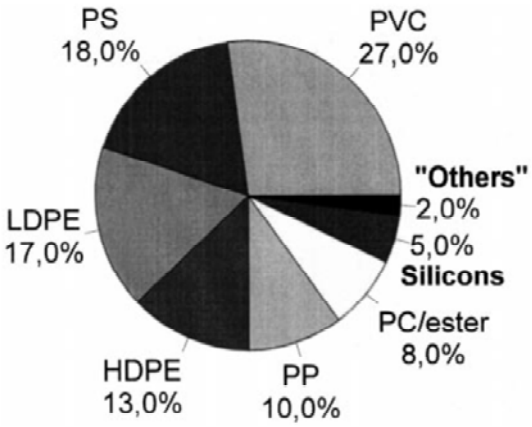

Figure 3-1. Synthetic polymers in medicine. [39]

PVC is polymerized from vinyl chloride monomer (VCM). As the VCM resin is heated or added with free radical initiator, the PVC polymerization proceeds primarily by a head-to-tail placement of the monomer units. The molecular structure is primarily $–CH_2-$ units alternating with –CHCl- units. The chlorine can be added on the previous chloride backbone, thus polymerizing to a bulk PVC.

For fabrication of plasticizer-PVC, a plasticizer, developed by the International Union of Pure and Applied Chemistry (IUPAC), can incorporates into PVC structure, increasing its flexibility, workability, and distensibility, or reducing the melt viscosity, the temperature of a scond-order transition and the elastic modulus of the product [40]. How plasticizers affect the PVC structure, or plasticization process, can be described by three theories: The *Lubricating Theory*, which the plasticizer monomer diffuses into the polymer and weaken the polymer-polymer interactive forces to prevent the formation of a rigid network as the system is heated, the *Gel Theory*, taking the plasticized polymer as intermediate state with a three-dimensional network of weak secondary bonding forces, and the *Free Volume Theory*, which the small plasticizer modifies the polymer backbone to create additional free volume. Overall, adding the plasticizer results in increased flexibility and softness of PVC. Furthermore, different plasticizers will exhibit different characteristics in the resulting mechanical and physical properties of the flexible product. Here in this study, we used Di(isononyl) Cyclohexane-1,2-Dicarboxylate (DINCH) as a plasticizer. The structure of DINCH is similar to those of the most used o-phthalates, diisononyl phthalate and di(2-ethylhexyl), but showing low environmental impact and low bio-toxicity (fig. 3-2) [41-42].

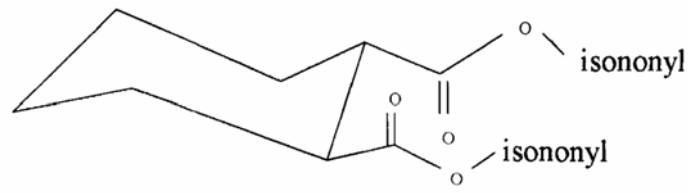

Figure 3-2. The structure of HEXAMOLL DINCH, Di(isononyl) Cyclohexane-1,2-Dicarboxylate. [42]

Another addictive has been added for PVC fabrication, called stabilizer. As initiating to heat the PVC mixer, the heat-released labile chlorine from PVC will attack the PVC backbone, causing the thermal degradation of PVC. Stabilizer prevents this to happen. Today, many mixed metal stabilizers for flexible PVC use zinc compounds, which exchange their anions to labile chorine atoms on PVC molecules. With backing up by barium or calcium, zinc octoate may increase the compatibility with PVC at higher temperature [40].

The PVC with high refractive index about 1.5 is suitable for SINAP system. Tuning the elastic moduli by plasticizers, the PVC can be adjusted to different stiffness, thus giving the application in biomechanical studies. Here, we cultured lung cancer cells on PVC substrates with different stiffness, and studied that how the filopodial dynamics are affected by the given rigidity stimuli with the advanced super-resolution microcopy, SINAP. In the following of this chapter, we will report the mechanical modulus, optical properties, and cell viabilities of the PVC substrates used in our experiments.

3.2 Materials and Methods

3.2.1 Substrate Preparation

The stiffness of PVC substrate was tuned by changing the ratio of a Plastic Hardener (M-F Manufacturing Co., Inc) and a carboxylate type plasticizer, DINCH (HEXAMOLL DINCH) developed by BASF, Ltd. (Yeou Yuan Trading co., LTD). The Plastic Hardener, DINCH and ZnBa heat stabilizer (Kindly provided by PAU TAI INDUSTRIL CORPORATION) were gently spun, dropped onto a regular coverslip (referred to as coverslip A), and degassed for 1 hour to expel bubbles. Another coverslip referred to as coverslip B was prepared by covering the coverslip with 1 ml of 0.1M NaOH solution for 5 min and then aspirated. As the surface of coverslip B dried, a 0.5 ml 3-APTES solution was spread on the NaOH-treated surface, incubated for 5 min, and the coverslip was rinsed with deionized water to remove excess 3-APTES [43]. Afterward the coverslip B was pressed onto the PVC mixture spun on the coverslip A, and the mixture was cured for 15min at 185°C in a vacuum oven (fig. 3-3). The coverslip A was removed after cooling the PVC mixture back to room temperature to yield a PVC-based substrate with flattened surface.

The fabrication of PA hydrogel mainly followed the protocol described by Tse and Engler [36]. Briefly, a mixture of 10% acrylamide and 0.3% bis-acrylamide

solutions was prepared, and polymerized with the addition of tetramethyl-ethylenediamine and 10% ammonium persulfate. The stiffness of resulting gel was measured to be 34.88 kPa using an atomic force microscope. The PDMS substrate was made by mixing a silicone elastomer (SYLGARD 184, Dow Corning) with the curing agent at a 10:1 ratio, degassed for one hour, spun on a regular coverslip, and cured at 65°C for 3.5 h, as advised by the manufacturer.

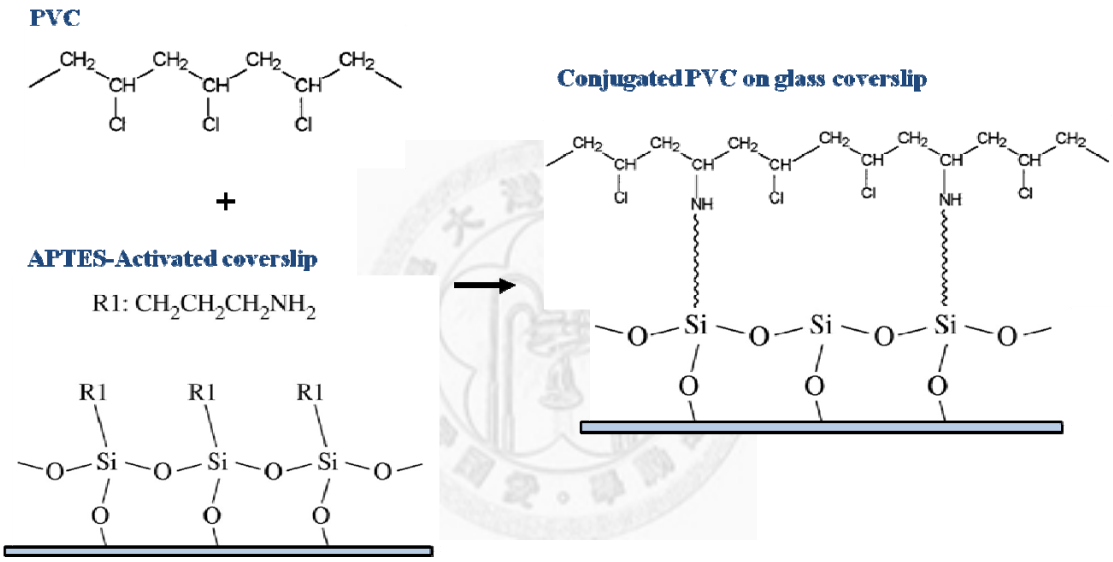

Figure 3-3. Conjugation of PVC onto the APTES-activated coverslips.

3.2.2 Cell Culture

Human lung adenocarcinoma cells CL1-5 cultured with Dulbecco's Modified Eagle's Medium supplemented with 10% fetal bovine serum and 1% antibiotic were used for this study. To facilitate cell adhesion to the substrates, the surface of the PVC-based and PDMS substrates were firstly steriled by UV light for 30 mins, then

coated with human fibronectin at a concentration of 50 μg/ml for one hour at room temperature, and finally blocked with 4% bovine serum albumin (BSA) at 4°C overnight [44]. The surface of the PA gel was coupled with 50 μg/ml fibronectin in HEPES solution with the aid of 0.2 mg/ml sufosuccinimidyl-6-(4'-azido-2'-nitro-phenylamino)-hexanoate (sulfo-SANPAH).

3.2.3 Cell Viability

Cell viability was measured by the MTT assay. The cells were then seeded onto the substrates at a concentration of 10^5 per ml and cultured at 37°C in a 5% CO_2 incubator. After 24 h of cell culture, the coverslips cultured with the cells were moved to new plates and treated with tetrazolium MTT (3-(4, 5-dimethylthiazolyl-2)-2, 5-diphenyltetrazolium bromide) for up to 2 h. The resulting intracellular purple formazan was solubilized by DMSO and quantified by light absorbance at 570 nm.

3.2.4 Substrate Stiffness

The bulk Young's modulus of the substrates was double-tested using a tissue deformation imaging stage and the MicroTester (Instron 8848) [45-46]. In the tissue deformation imaging stage testing, a cube of the substrate with 8mm in length and

4.5mm in thickness was prepared and secured between two metal plates mounted on a confocal microscope. One of the metal plates was connected with a computer-controlled PZT plate. Sinusoidal deformations up to 1—3% of the initial thickness of the sample were exerted on the held substrate by the PZT plate. The strain of the sample was measured from the confocal images and the stress was obtained from the PZT plate (fig. 3-4). The Young's modulus was then calculated from the linear fit for the stress and strain curve. In the MicroTester testing, the same-sized cube sample was fixed on a stationary load cell, which recording the stress of the sample, and applied a compressive forces by a piston to generate the sample a static displacement by 1.75μm (about 0.03% sample thickness) (fig. 3-5). The Young's modulus was calculated from the linear fit for the stress and strain (between 5% and 10%) curve.

3.2.5 Refractive Index Measurement

The refractive index of the PVC-based substrates was quantified using phase contrast tomography [47]. In brief, the substrates were patterned on lines with 6μm in depth and covered by a glycerol solution for the reference of refractive index. A laser beam of 405 nm in wavelength was shined to the sample and a reference beam was separated by a beamsplitter. The interference images between the reference light and that transmitting the sample were acquired by a CCD camera at a frame rate of 470 per

second. The refractive index of the substrate was then calculated based on the phase difference of the images (fig. 3-6).

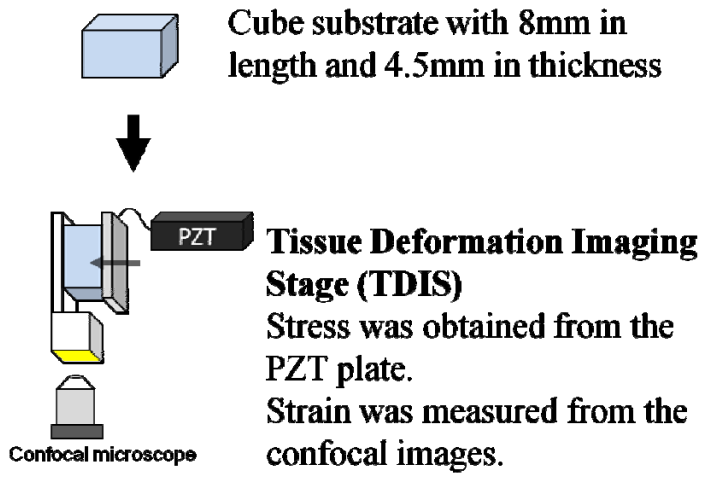

Figure 3-4. The experiment flow of TDIS testing.

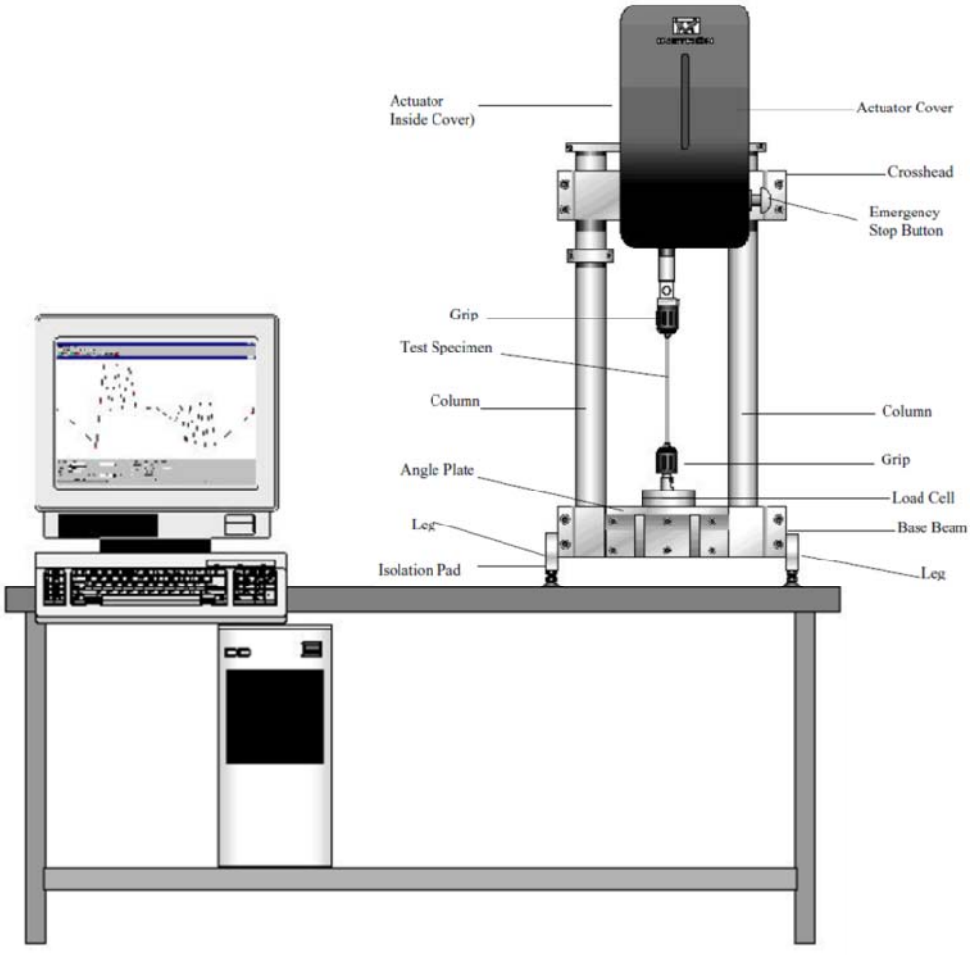

Figure 3-5. Typical test system configuration of MicroTester. [46]

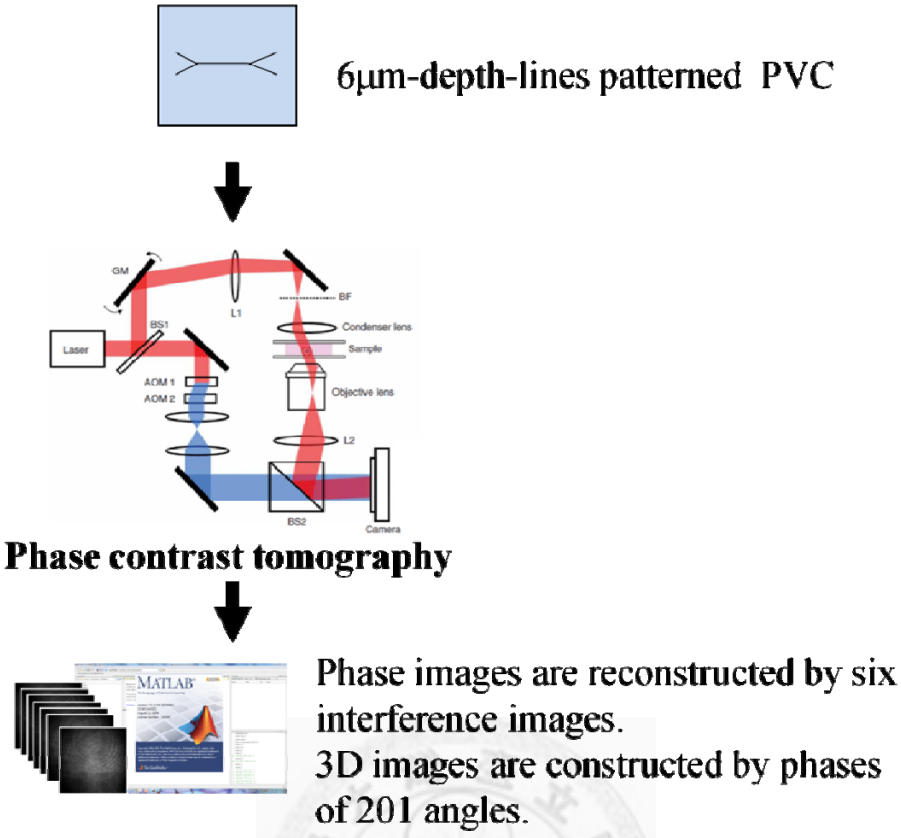

Figure 3-6. The experiment flow of refractive index measurement.

3.3 Result

3.3.1 Cell viability

MTT assays were conducted for cells cultured on PVC-based, PA gel, and PDMS substrates respectively. Cells cultured on regular coverslips were used as control. The result showed that the growth of the CL1-5 cells on PA gel was the best, with an averaged viability of 63.5% (range: 60—67%). The averaged viability of cells grown on the PVC composites and the PDMS substrates were similar, ranging from 30% to 50%, slightly lower than that for PA gels (fig. 3-7). Such differences may result from the

variation of approaches adapted for coupling the fibronectin onto the substrate surface. The proteins were chemically conjugated to the gel surface and may preserve the greatest biofunctionality. In contrast, the proteins were physically absorbed to the PVC and PDMS surfaces to reduce the fluid surface tension exerted on the substrate surface, which should result in conformation change of the proteins and consequently deteriorate the functionality. Nevertheless, the similar results between the PVC composites and the PDMS substrates suggest that the former may be a good candidate for various bioMEMS relevant studies.

3.3.2 Substrate stiffness

It is well known that mammalian cells can sense and response to compliant substrates, while the stiffness of various tissues ranges from several kPa to hundreds kPa [5, 27, 48]. For example, the Young's modulus of skeletal muscles is about 8—17 kPa and that of precalcified bone is about 25—40 kPa [49]. The Young's moduli of the PVC composites with various ratios between the PVC and the softener, were 60 kPa, 35 kPa, and 20 kPa, for the mixture ratio of 3:1, 2:1, and 1:1, respectively, compatible with the physiological range of tissue stiffness (fig. 3-8).

3.3.3 Optic properties

The refractive indices of PVC and the plastic softener were measured to be 1.53—1.57 and 1.47, respectively. The resultant refractive indices of the PVC composite hence varied from 1.47 to 1.53, very close to that of glass and much higher than that of PA gel (~1.33) and PDMS (~1.44) (fig. 3-9). These results suggest that PVC-based substrates are suitable for SINAP-related studies.

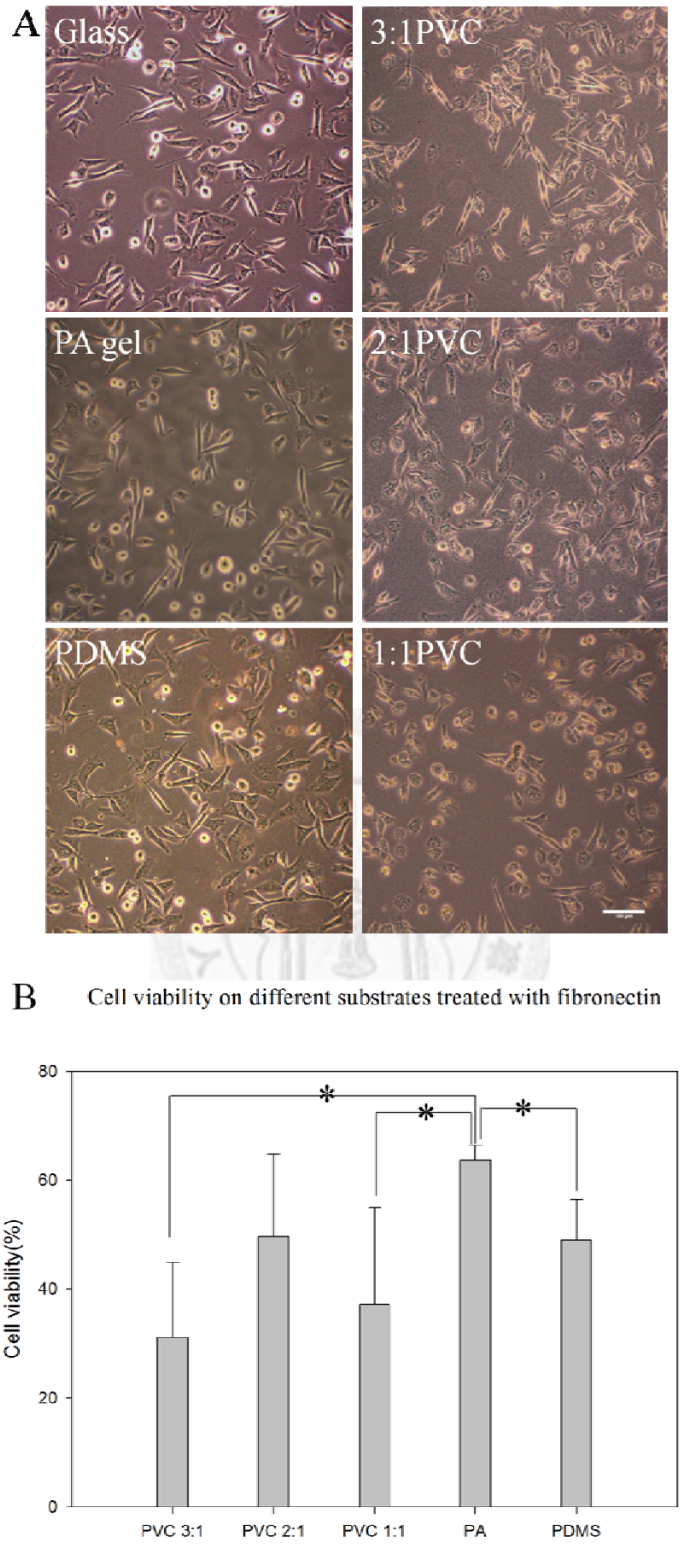

Figure 3-7. (A) Phase contract images of CL1-5 grown on different substrates. (Scale bar=100 μ m) (B) The averaged viability ratios for cells grown on different substrates. Error bars represent standard deviation. (n=6) * $P < 0.05$

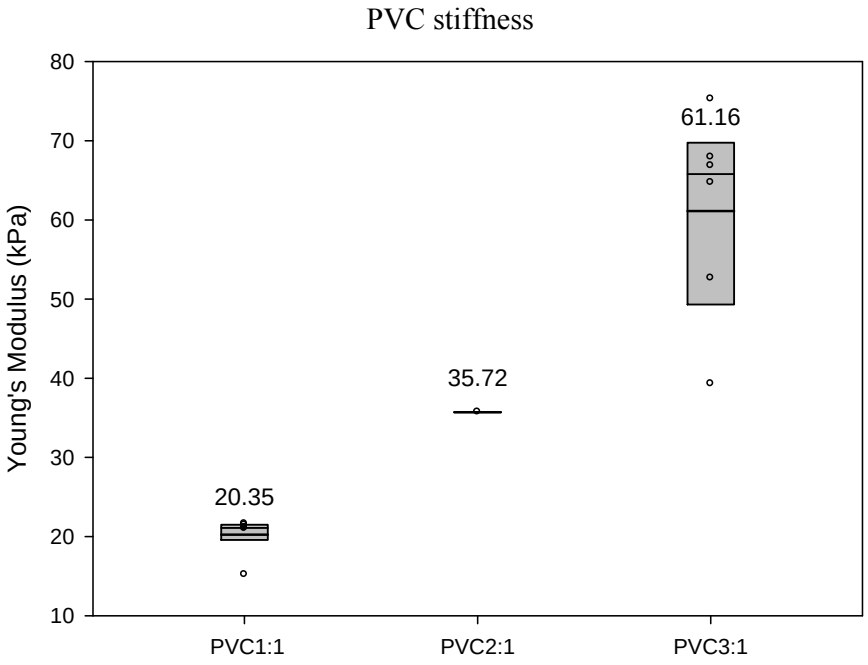

Figure 3-8. The mean Young's modulus of the PVC composite with various ratios of PVC and the softener. Error bars represent standard deviation. (*n*=6 for PVC1:1 and PVC3:1, n=1 for PVC2:1).

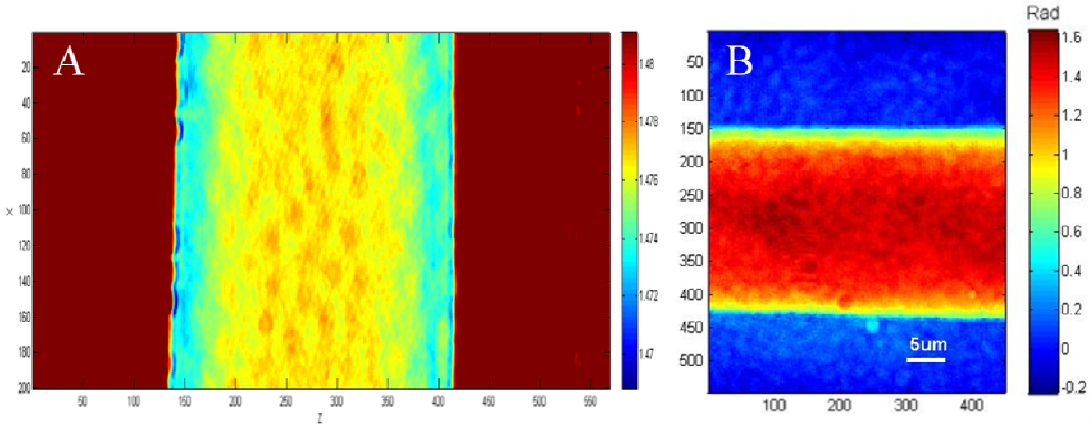

Figure 3-9. The resultant refractive indices of the PVC. (A) Phase images calculated by 2D tomographic phase microscope. (B) Refractive index calculated by 3D tomographic phase microscope.

3.4 Conclusion

Poly(vinyl chloride) (PVC) is one of the widely used polymers for industrial and biomedical applications due to its light weight, easy processing, and low manufacturing cost. There are various methods to modify the surface of the PVC film such as chemical treatment, plasma treatment, glow discharge, and ion irradiation in order to improve the biocompatibility [44, 50]. We examine the cell viability of PVC-based substrates, which is chemically treated by coating fibronectin. Cells grown on fibronectin-coated PVC substrate was found to be better than other ECM protein (such as gelatin and collagen) [44]. Our results show that cell number is no less on PVC than on PDMS and no different between PVC with ratio of 3:1, 2:1, and 1:1, which indicating that the surface properties do not change by composition of Hardner and Softner.

Our study further demonstrates the optical properties and mechanical properties of elastic PVC with different ratio of the Hardner to the Softner. The property with high refractive index may improve some optical techniques: SINAP is one example that we performed, and total internal reflection fluorescence (TIRF) microscopy may be another. TIRF microscopy is an ideal technique for interrogating the cell-substratum interface with contrastive refractive indices, thus the optical properties of the substrate are considered requirements. Several materials, such as PDMS and PVMS, have been used to TIRF microscopy, but their elastic modulus are much higher than the physiological

range of tissue stiffness [51]. PVC may be compatible to TIRF microscopy because its refractive index is close to glass (1.47-1.53) and the elastic modulus is fitting to the physiological condition (E = 18-60 kPa).

In conclusion, with tunable stiffness and high refractive index, we can exert SINAP technique on cells grown on PVC, improving the resolution of images. In the next chapter, we monitor the detail morphological response of a living lung cancer cell to the mechanical stimulation from environment.

Chapter 4 Experimental Procedures for Filopodia Observation

4.1 SINAP System Setup

The SINAP system was composed of a standard upright microscope (Eclipse LV150, Nikon, Kanagawa, Japan) equipped with a water-immersion objective with a 1.1 numerical aperture (CFI Plan 100×W, Nikon). The illumination wavelength was set as 550 nm with a bandwidth of 200 nm. The illumination patterns were generated by a liquid-crystal spatial light modulator (SLM) (HEO 6001-SC-II, HOLOEYE Photonics, Berlin-Adlershof, Germany). Images were captured by a 14-bit electron-multiplying CCD camera (DU-885, Andor, Belfast, Northern Ireland), which cooled down at -60°C to reduce noise. Axial positioning of the sample was controlled by a PZT-driven vertical stage (P-762.ZL, Physik Instrumente, Karlsruhe, Germany) that has a 10-nm smallest step size and 0.1% linearity (fig. 4-1) [34].

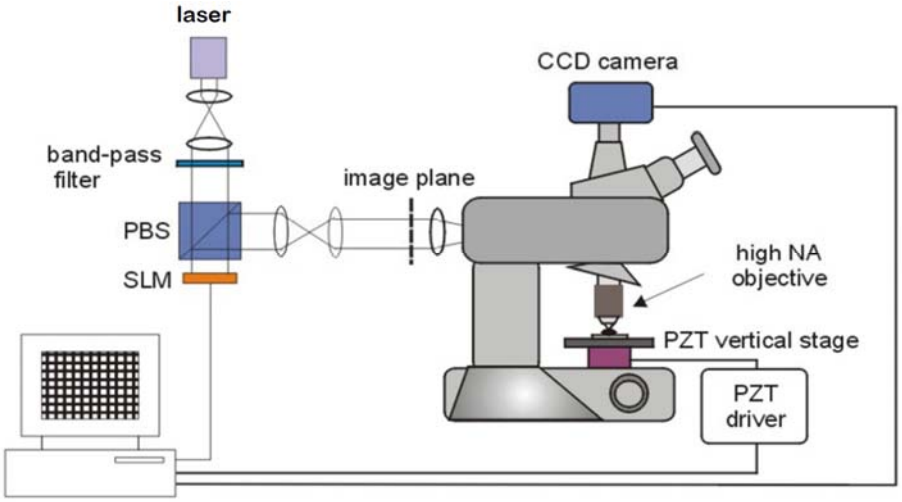

Figure 4-1. The setup of SINAP system. [34]

A laser beam firstly passed through a diffuser to decrease the spatial coherent of the laser beam. If the laser beam has high spatial coherent, the images will be interfered by the speckle. The wavelength of the laser beam was then filtered between 550nm and 750nm by two bandpass filters due to the phototoxicity of UV light and the heat of the infrared ray. After the polarization beam splitter (PBS) separated the P wave and the S wave of the laser beam, only the P wave could pass through the PBS and project on the SLM. The SLM here was connected to a computer and as a phase modulator, which could shift the phase with higher speed (about 60 Hz per second). The modulated pattern was illuminated on the image plane and projected onto the specimen by the 4f system of the standard upright microscopy. Under this setup, the spatial frequency of the modulating mesh pattern on the sample surface was about 2 μm^{-1}, and every pixel on the image was equaled to 140 nm in reality.

For live-cell experiment, the microscopy was located in a 37°C incubator to keep the cell-cultured temperature (fig. 4-2). Moreover, the accurate temperature controlling could reduce the noise from the thermal expansion of the PZT-driven vertical stage.

The system was setting up by the Kao, Yu-Chiu. The calibration process was conducted by LABVIEW and MATLAB programs developed by Dr. Lee's group.

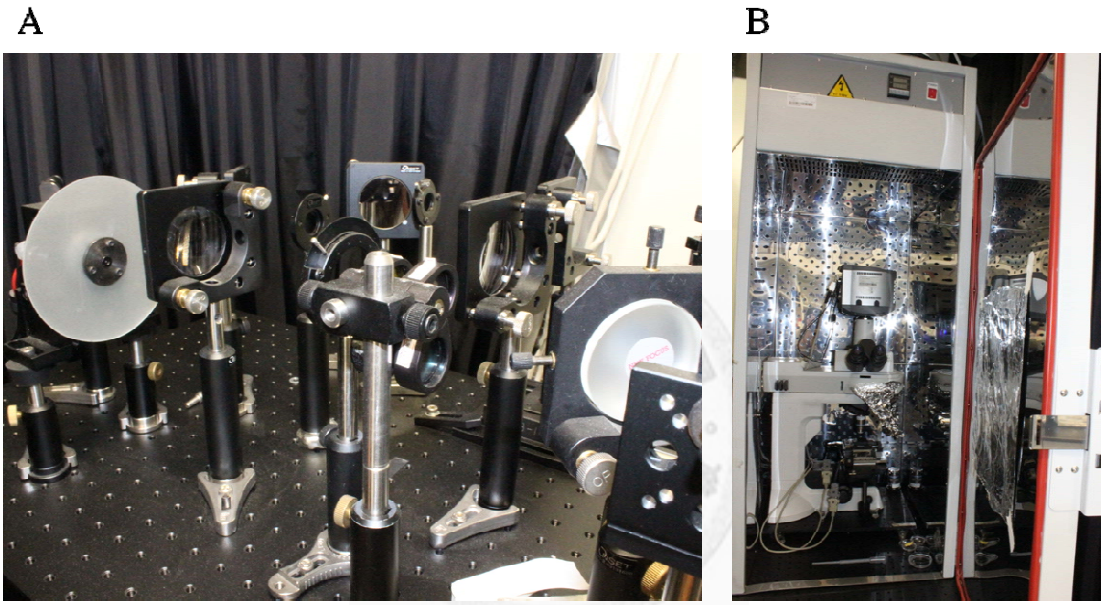

Figure 4-2. (A) The SINAP system in Kuo's lab. (B) A standard upright microscope in a 37°C incubator.

4.2 Cell-Cultured Chip Preparation

The cell-cultured PVC substrates and cell line were described as the previous chapter. For long-time observation, the cell-cultured system was enclosed into a closed chip (fig. 4-3). A one-mm-thick acrylic sheet was cut a central hollow with 3.5 mm in length and 2.2 mm in width and fixed onto a 10-cm cultured dish. The PVC substrate

made onto an 18x18 coverslip was placed into the central hollow. The CL1-5 cells were then seeded onto the substrates at a concentration of 10^4 per ml and cultured at 37°C in a 5% CO_2 incubator for 24 h before further experiments. Before SINAP observation, the central hollow was covered by a 24 x 60 coverglass to avoid contaminant and maintain the medium osmotic pressure.

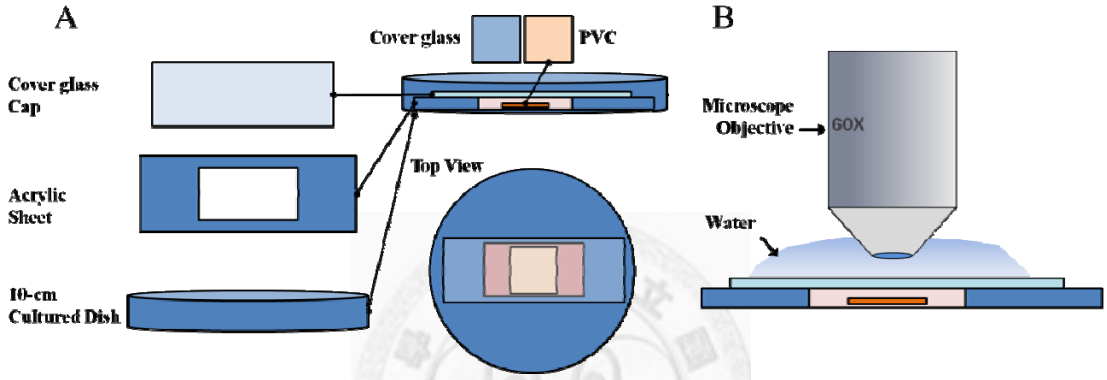

Figure 4-3. (A) The design of the closed chip. (B) The closed chip in the SINAP system. For the water-immersion objective, diH_2O was dropped onto the cover glass cap, and the objective directly immersed into the water.

4.3 Drug Treatment

For myosin II inhibition, blebbistatin (Sigma-Aldrich) was used at a concentration of 30μM. Because blebbistatin is sensitive to radiation below 500 nm, live-cell images were taken between 550 nm and 750 nm as above. After the cells were seeded on the PVC substrates and cultured for 24 hours, the medium was sucked and drug-contained medium was added into the chip. Cells were treated with drug for one hour before SINAP observation.

4.4 Immunofluorescence

Cells were fixed for 10 mins in 4% paraformaldehye, permeabilized for 5 mins in 0.01% Triton X-100, and blocked with 1% bovine serum albumin (BSA) for 1 hr at room temperature. For vinculin staining, cells were incubated with primary antibodies (1:200 rabbit polyclonal vinculin antibody in blocking solution; Gene Tex®, Inc.) overnight at 4°C, and incubated with fluorophore-conjugated secondary antibodies (1:250 Alexa Fluor 488 goat anti-rabbit in blocking solution; Invitrogen) for 2 hr at room temperature. Cell nuclei were stained using 4',6'-diamidino-2-phenylindole (DAPI) dye for 10 mins. Finally, the samples were mounted on slide in mounting media (Dako) and sealed with nail polish.

4.5 Confocal Images acquisition

Images of the CL1-5 cells were acquired using a laser scanning confocal microscope (LSM 510 Meta, or LSM 710, Zeiss, Germany) with an 100× objective lens (Plan-Apochromat Oil M27, NA 1.4, Zeiss). Series of z-stack images or single image were taken from the focal plane of vinculin staining. The Zen 2009 Light Edition software (v5.5.285.0, Zeiss) was used to adjust image intensity and contrast.

4.6 Data analysis

Statistical analyses were performed using SigmaPlot^{TM} (Systat Software Inc., CA). We evaluated the parameters with Student's t-test to compare the difference between differ experimental groups. For this study, a value of $p < 0.05$ was considered significant.

Chapter 5 Results

5.1 High-Refractive-Index PVC Substrates under the SINAP

SINAP, as demonstrated previous, with nanometer depth and lateral resolution was advanced in the observation of filopodial dynamic, while the substrates under the observed sample should have high refractive index. Besides, for our speculation, which the filopodial dynamic would be related to the matrix rigidity, the substrates should have tunable stiffness. Based on the above limitation, we cultured lung cancer cells CL1-5 on the PVC substrates for SINAP application. Figure 5-1 illustrated SINAP images and bright field images of a CL1-5 cell cultured on PVC substrate with the ratio of the Hardener to the Softener as 3:1 and 1:1 respectively. The yellow arrow highlights a filopodium in the SINAP image, which is barely seen in the bright-field image. Supported by the SINAP, we could quantify the filopodial density and stretching rate of CL1-5 more accurately.

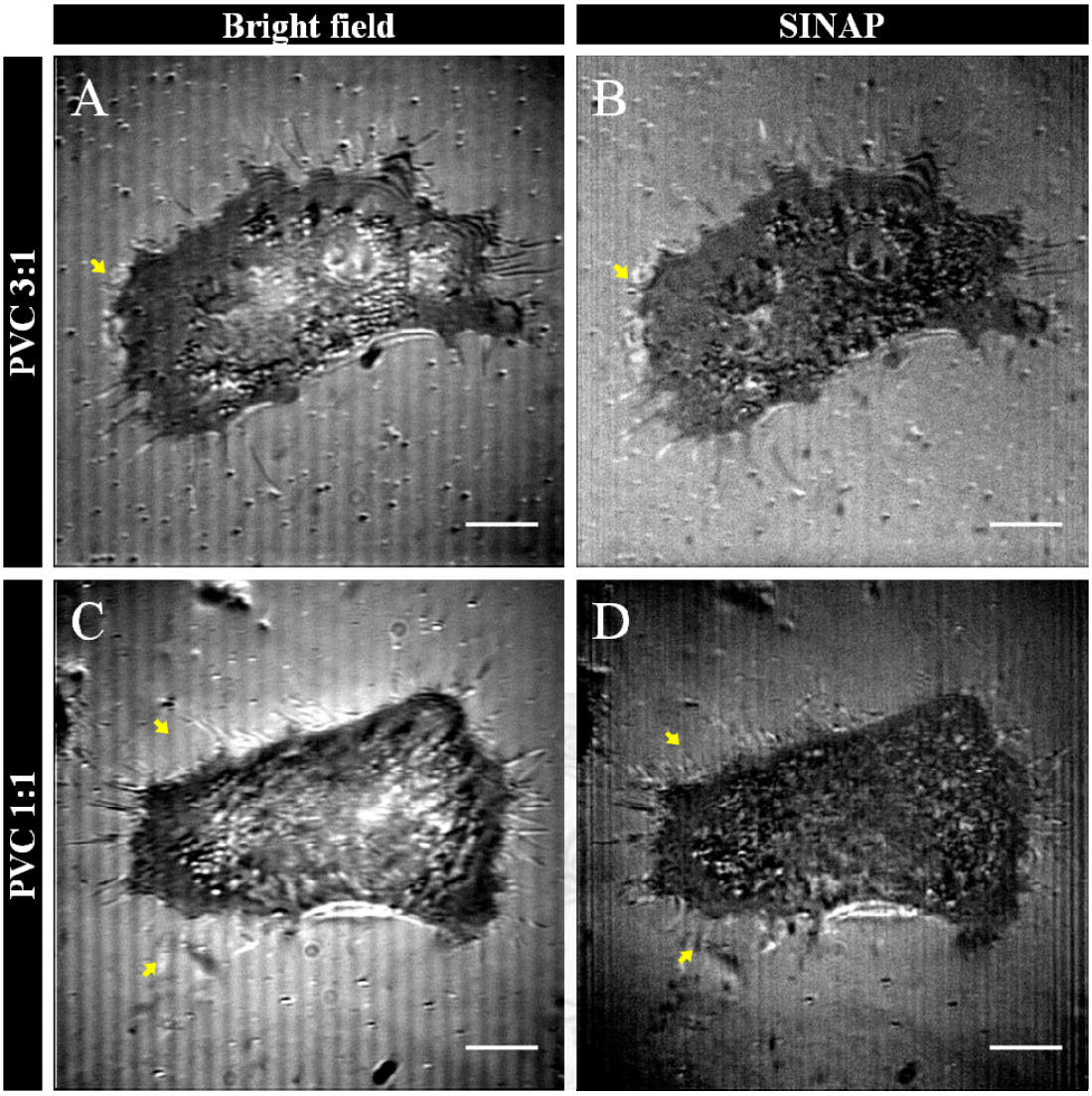

Figure 5-1. Comparison between a bright-field image (A, C) and a SINAP image (B, D) for a CL1-5 cell cultured on PVC substrate with the ratio of the Hardener to the Softener as 3:1 (A-B) and 1:1 (C-D). The yellow arrows highlight filopodia in the SINAP image, which is barely seen in the bright-field image. (Scale bar = 10 μm)

5.2 Filopodia Density and Length on Substrates with Different Stiffness

The lung cancer cells CL1-5 were seeded onto the PVC substrates with hardner and softner at the ratio of 3:1 and 1:1, whose Young's modulus were about 60 kPa and 20 kPa respectively. The filopodial number and length of CL1-5 were quantified by Image J from SINAP images. The filopodial number was normalized by the perimeter of the cell, represented as "filopodia density". Figure 5-2 shows the filopodia density of CL1-5 under PVC1:1, PVC 3:1 and glass. The results reported that the cells cultured on the soft substrate, whose Young's modulus was about 20 kPa, had higher filopodial density (filopodial density = 0.55 number per μm, n = 33) than those cultured on the PVC 3:1 substrate (Young's modulate = 60 kPa, filopodial density = 0.308 number per

n = 18, $p = 4.4\times10^{-9}$) and the glass (Young's modulate = MPa, filopodial density = 0.311 number per μm, n = 20, $p = 2.7\times10^{-9}$).However, the filopodial density had no significant difference between the PVC3:1 substrate and the glass (p = 0.915). Besides, the filopodial length on the soft substrates was longer than those on the stiff substrate (fig 5-3) ($p = 3.643\times10^{-4}$ for comparison of the PVC3:1 and $p = 5.071\times10^{-3}$ for comparison of the glass), while the filopodial lengths were not different between the

PVC3:1 substrate and the glass (p = 0.599). These results agree with previous study [29], and we further quantified the striking difference here. Furthermore, this difference might be the result of different adhesive strength, which has been shown to involve in the rigidity sensing system, between the filopodia and the substrate. Thus we traced the stretching rate of the filopoida in the next section.

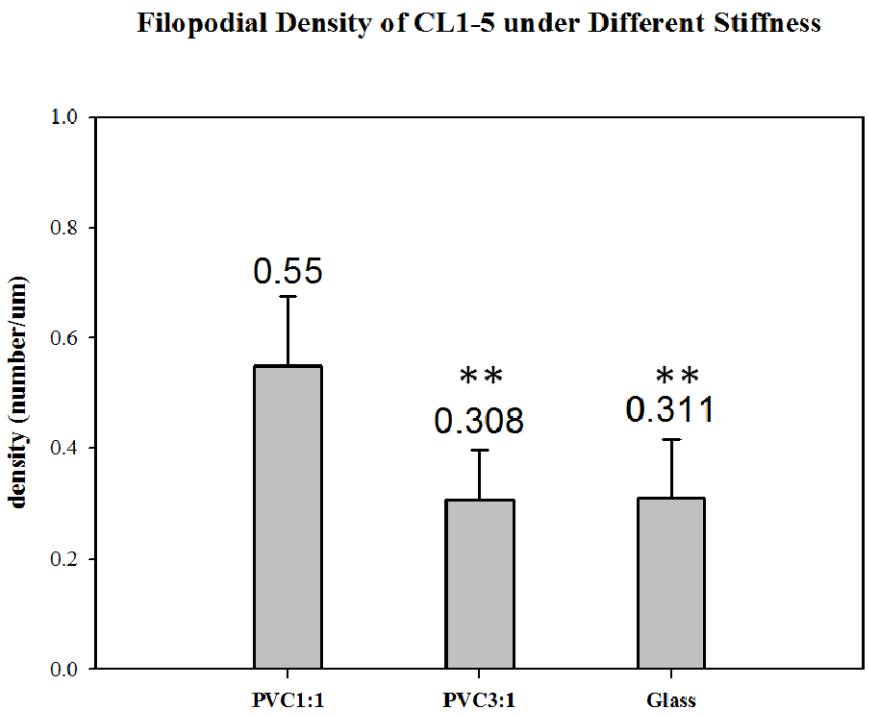

Figure 5-2. Effects of substrate stiffness on the filopodial density. Numbers above each bar represent the mean of filopodial density. Error bars indicate 95% confidence interval of the mean. Statistical cell number = 33, 18, and 20 for PVC1:1, PVC3:1, and Glass, respectively. ** $P < 0.01$.

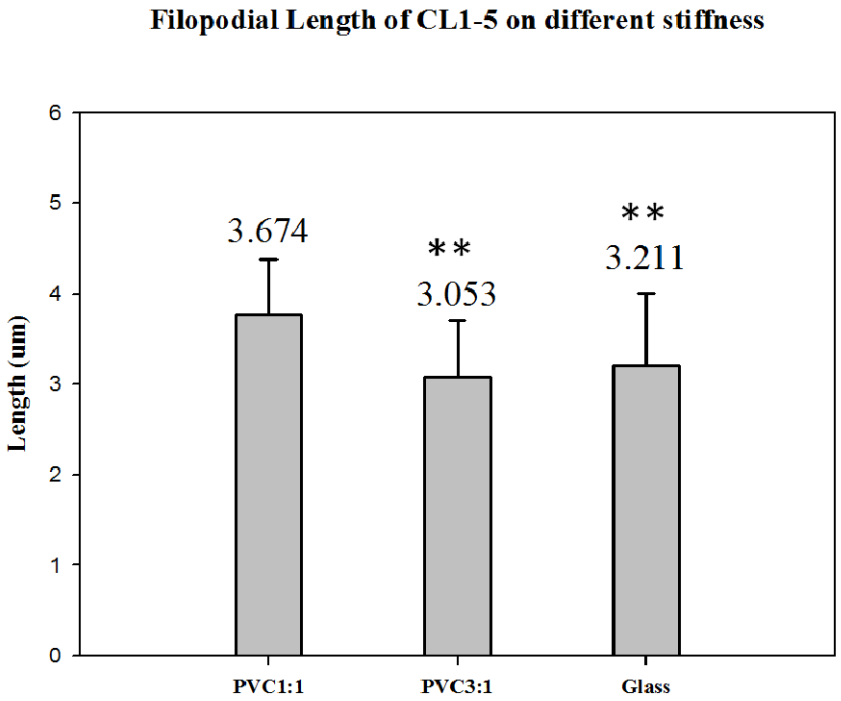

Figure 5-3. Effects of substrate stiffness on the filopodial length. Numbers above each bar represent the mean of filopodial length. Error bars indicate 95% confidence interval of the mean. Statistical cell number = 33, 18, and 20 for PVC1:1, PVC3:1, and Glass, respectively. ** $P < 0.01$.

5.3 Stretching Rate of Filopodia on Substrates with Different Stiffness

To clarify the mechanism of the difference in filopodial density and length between different stiffness, the stretching rate of the filopodia was quantified from the time-lapse images. We recorded the length of a filopodia every ten seconds for five minutes and portray the dynamic track of the changing length by MATLAB program (fig. 5-4 (a-c)). However, it was hard to compare the dynamic tracks of three groups, thus we further

quantified the stretching rate of the filopodia. According to previous studies, the protrusion rate and the retraction rate could be separated. The protrusion rate might not be affected by the matrix rigidity, since integrins at the leading edge of the filopodia were not yet attached to ECM ligands. Conversely, the retraction of filopodia would mediate the rigidity sensing as the focal adhesion had formed at the filopodial tips [26]. Therefore, in our analysis, we found out the peaks and valleys of each track (fig. 5-4 (d-f)), and calculated the protrusion rate or retraction rate between the adjacent peak and valley (fig. 5-4 (g-l)).

Figure 5-5 shows the results of the protrusion rate and the retraction rate of filopodia of CL1-5 on substrates with different stiffness. The filopodial protrusion rate of CL1-5 on the soft PVC1:1 substrate (protrusion rate = 0.051μm per second) was slightly slower than that on the stiff PVC3:1 substrate (protrusion rate = 0.054μm per second, $p = 0.037$) but not different from that on the glass (protrusion rate = 0.061μm per second, $p = 0.528$). However, the filopodial retraction rate of CL1-5 on the soft PVC1:1 substrate (retraction rate = -0.051μm per second) was a little slower than that on the glass (retraction rate = -0.065μm per second, $p = 0.041$) but not different from that on the stiff PVC3:1 substrate (retraction rate = -0.053μm per second, $p = 0.820$). Moreover, there were no differences in whether the protrusion rate or the retraction rate

between PVC3:1 group and glass group (p = 0.326 for comparison in protrusion rate and p = 0.114 for comparison in retraction rate).

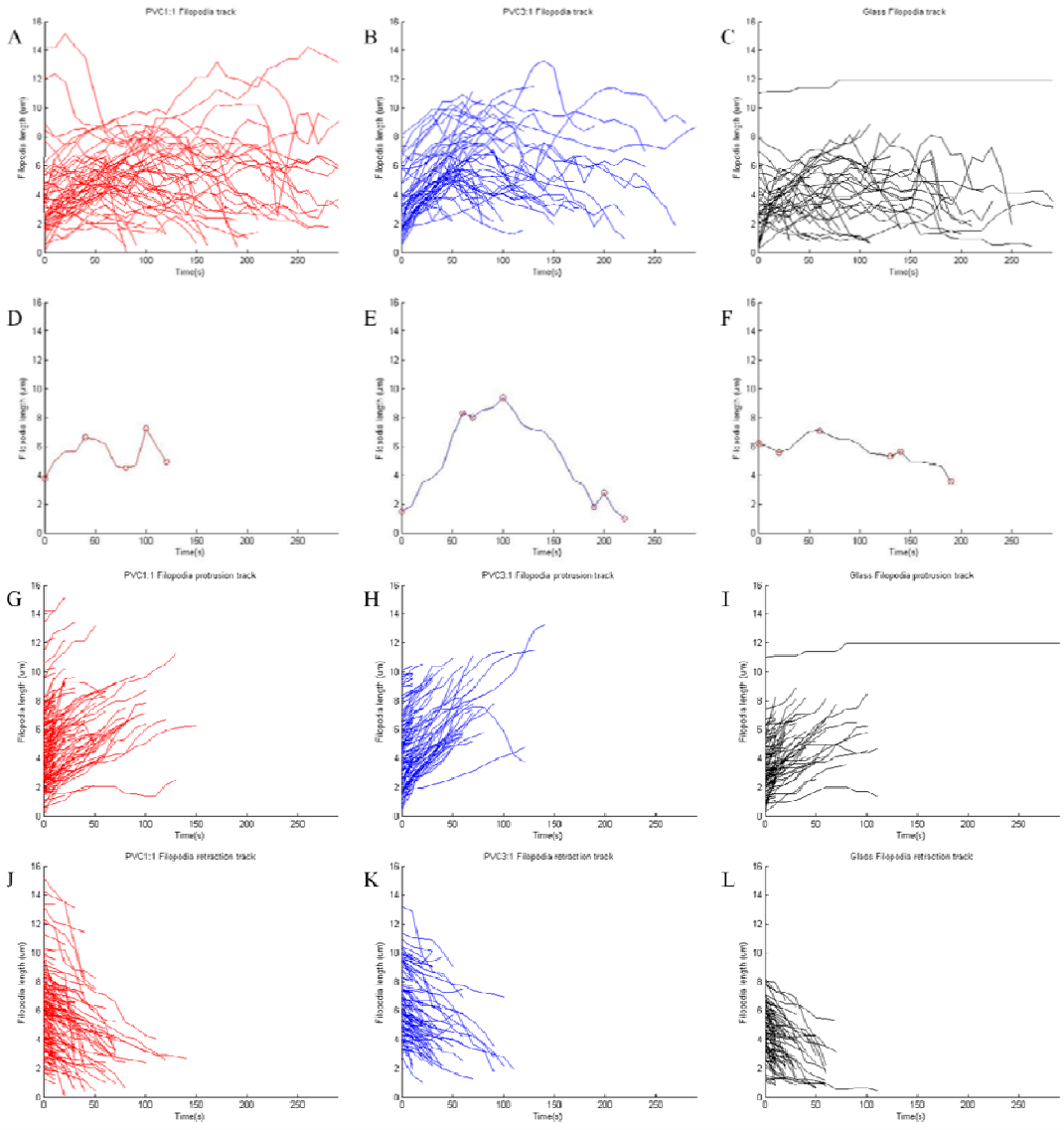

Figure 5-4. The data processing. (A-C) The raw data of filopodia tracking. Red lines represent the cells cultured on PVC1:1; blue lines represent the cells cultured on PVC3:1; black lines represent the cells cultured on glass. (D-F) Schematic diagram of data processing. The each demonstrated line is one of the filopodial track. The red circles indicate the found peaks and valleys. (G-I) The protrusion tracks of the filopodia. (J-L) The retraction tracks of the filopodia. Statistical filopodia number = 51, 50, and 34 for PVC1:1, PVC3:1, and Glass, respectively.

The forming of tip complex to connect the filopodia and the substrate is related to the length of the filopodia. Therefore, we grouped the filopodia with different lengths and calculated their protrusion rate and retraction rate again. The demarcation length was defined as the median length of all the traced filopoida, and was four μm. Figure 5-6 shows the re-calculated results of the protrusion rate and the retraction rate of filopodia of CL1-5 on different stiffness with different starting length. After grouping with the filopodial length, comparisons of the protrusion rates, whether between different stiffness but the same starting length or between the different starting but the same stiffness stimulation length, were no significant difference (fig. 5-6 (a)) (p values were shown as the below).

P value		PVC 1:1		PVC 3:1		glass	
		>4	<4	>4	<4	>4	<4
PVC 1:1	>4	-	0.766	0.241	-	0.717	-
	<4	-	-	-	0.066	-	0.314
PVC 3:1	>4	-	-	-	0.737	0.297	-
	<4	-	-	-	-	-	0.578
glass	>4	-	-	-	-	-	0.425
	<4	-	-	-	-	-	-

On the other hand, the retraction rate was slightly slower as the filopodia was shorter in the PVC 1:1 experiment. It also showed that the short filopodia of cells on the PVC1:1 retracted more slowly than those short filopodia of cells on the glass, and the

long filopodia of cells on the PVC3:1 retracted more slowly than those long filopodia of cells on the glass (fig. 5-6 (b)) (p values were shown as the below).

P value		PVC 1:1		PVC 3:1		glass	
		>4	<4	>4	<4	>4	<4
PVC 1:1	>4	-	0.002	0.637	-	0.055	-
	<4	-	-	-	0.325	-	0.009
PVC 3:1	>4	-	-	-	0.356	0.040	-
	<4	-	-	-	-	-	0.376
glass	>4	-	-	-	-	-	0.057
	<4	-	-	-	-	-	-

However, these differences in stretching rate showed no correlation to the differences in filopodial density and length of CL1-5 on different stiffness, as demonstrated in section 5-2. Therefore, the different density and length of filipodia resulted from the different stiffness stimulation should be controlled by other mechanism.

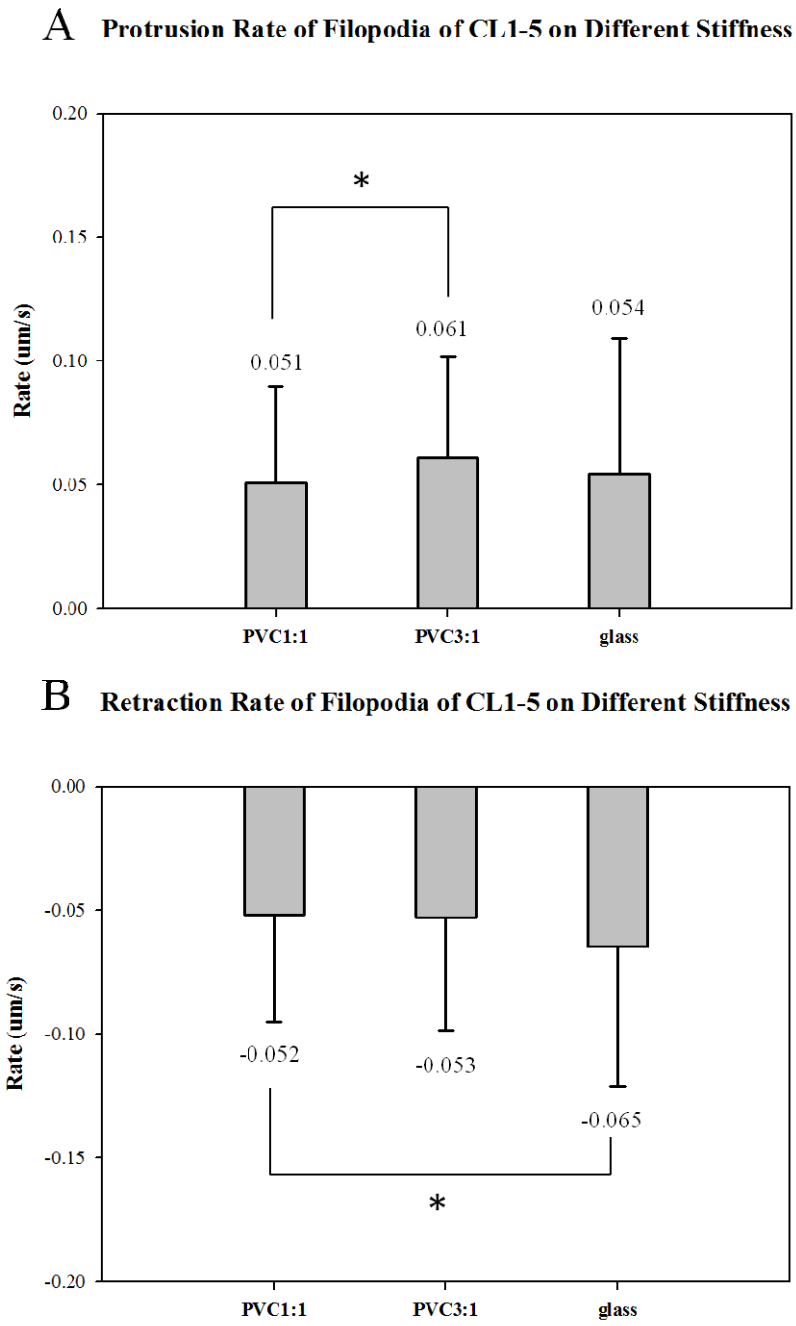

Figure 5-5. (A) The protrusion rate of the filopodia of CL1-5 on substrates with different stiffness. (B) The retraction rate of the filopodia of CL1-5 on substrates with different stiffness. Numbers above each bar represent the mean of protrusion rate. Error bars indicate 95% confidence interval of the mean. * $P < 0.05$.

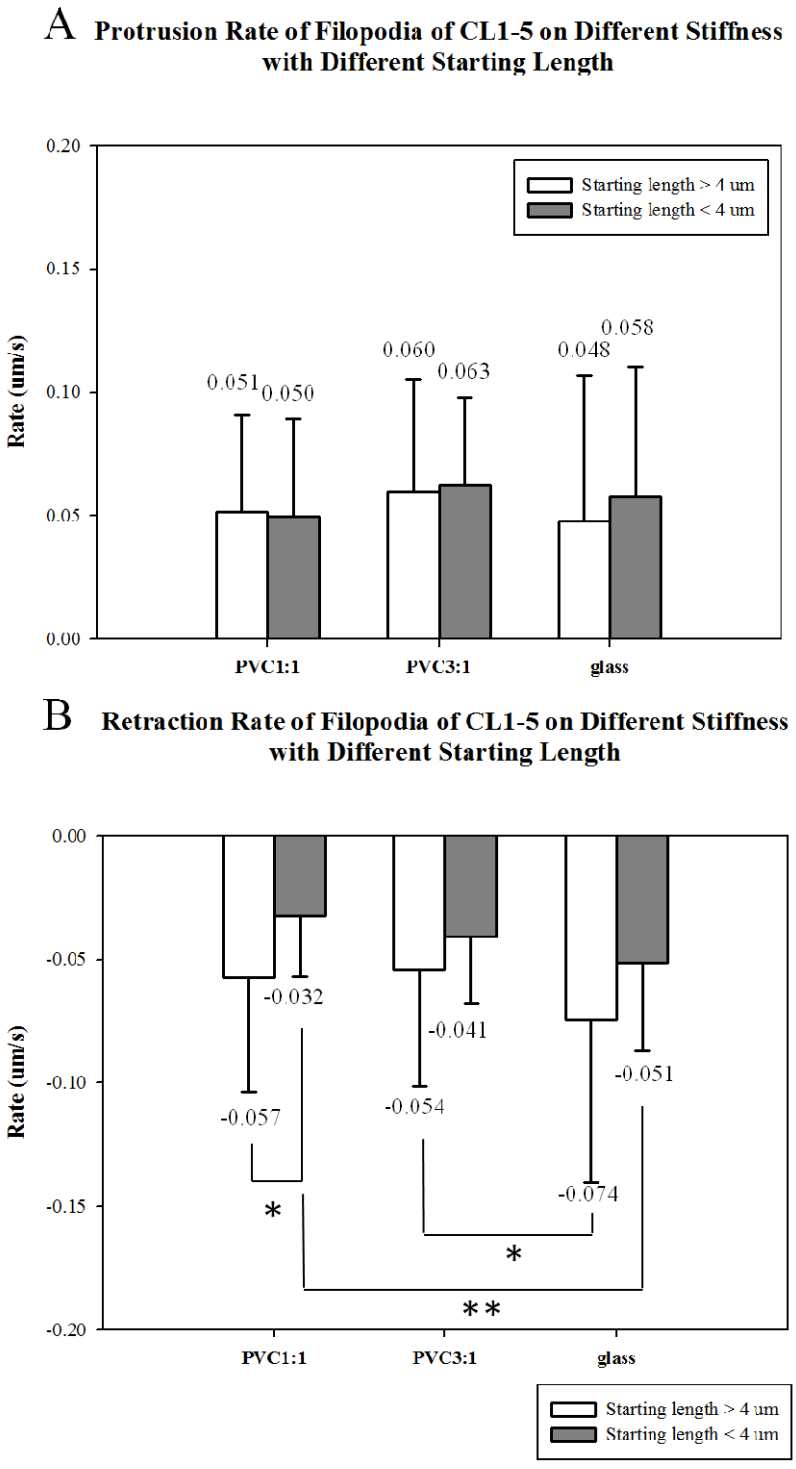

Figure 5-6. (A) The protrusion rate of the filopodia of CL1-5 on substrates with different stiffness. (B) The retraction rate of the filopodia of CL1-5 on substrates with different stiffness. The white bars represent that the starting length of filopodia is longer than 4μm, while the dark-gray bars represent that the starting length of filopodia is shorter than 4μm. Numbers above each bar represent the mean of protrusion rate. Error bars indicate 95% confidence interval of the mean. * $P < 0.05$. ** $P < 0.01$.

5.4 Filopodial Density and Length on Substrates with Different Stiffness with Blebbistatin Treatment

The forming of filopodia has been shown to be against to the stress fibers, since the high cellular level of active Rac expressing, which down-regulated the formation of filopodia, is often correlated with the low level of Rho, the stress fibers enhancing proteins [28]. It has been reported that stiff substrates stabilize integrin focal adhesion clusters and enhance the contractility and the formation of the stress fibers [29]. Therefore, we speculated that the increase in filopodial density and length might be correlated with the inhibition of Rho-induced stress fiber formation and stability when the cells were cultured on the soft substrates. To exam this speculation, the cells cultured on different stiffness were treated with 50 μM blebbistatin, a myosin II inhibitor, for one hour before observed under SINAP. The maturation of focal adhesions was checked by staining of vinculin, a focal adhesion protein (fig. 5-7). From the images of those without treatment, we could see that cells had more mature focal adhesions (green punta) on stiff substrates than on soft substrates. After the blebbistatin treatment, the focal adhesions decreased on three substrates. Figure 5-8 shows the results of filopodial density of CL1-5 on different stiffness before and after the treatment with blebbistatin. After treated with blebistatin, the filopoidal densities of

CL1-5 on all range of stiffness dramatically increased (n = 10, p = 0.046 for PVC1:1, n = 13, p = 2.112×10^{-6} for PVC3:1, and n =10, p = 0.006 for glass). The more striking result with the blebbistatin treatment was that the difference in filopodial density between cells on soft (PVC 1:1) and on stiff (PVC3:1) substrates was disappeared (p = 0.091). Although the filopodial density of cells on glasses was slightly lower than those on soft substrates (p = 0.014), the difference in the experiment with blebbistatin treatment was reducing comparing to that without blebbistatin treatment.

We also compared the filopodial length of cells on different stiff after blebbistatin treatment (fig 5-9). The results revealed that the filopoida of cells on stiff (PVC3:1) substrates and glass were longer after the treatment, while the filopoidal length of cells on soft (PVC1:1) substrate remained steady (n = 10, p = 0.484 for PVC1:1, n = 13, p = 0.005 for PVC3:1, and n =10, p = 1.163×10^{-4} for glass). However, comparing the filopodial length after the blebbistatin treatment, there was no manifest difference between substrates with different stiffness (p = 0.982 for comparison between PVC1:1 and PVC3:1, p = 0.112 for comparison between PVC1:1 and glass, and p = 0.066 for comparison between PVC3:1 and glass). In other words, it could imply that the treatment with blebbistatin on stiff substrates (PVC 3:1 and glass) would mimic the situations which the cells met on the soft substrates.

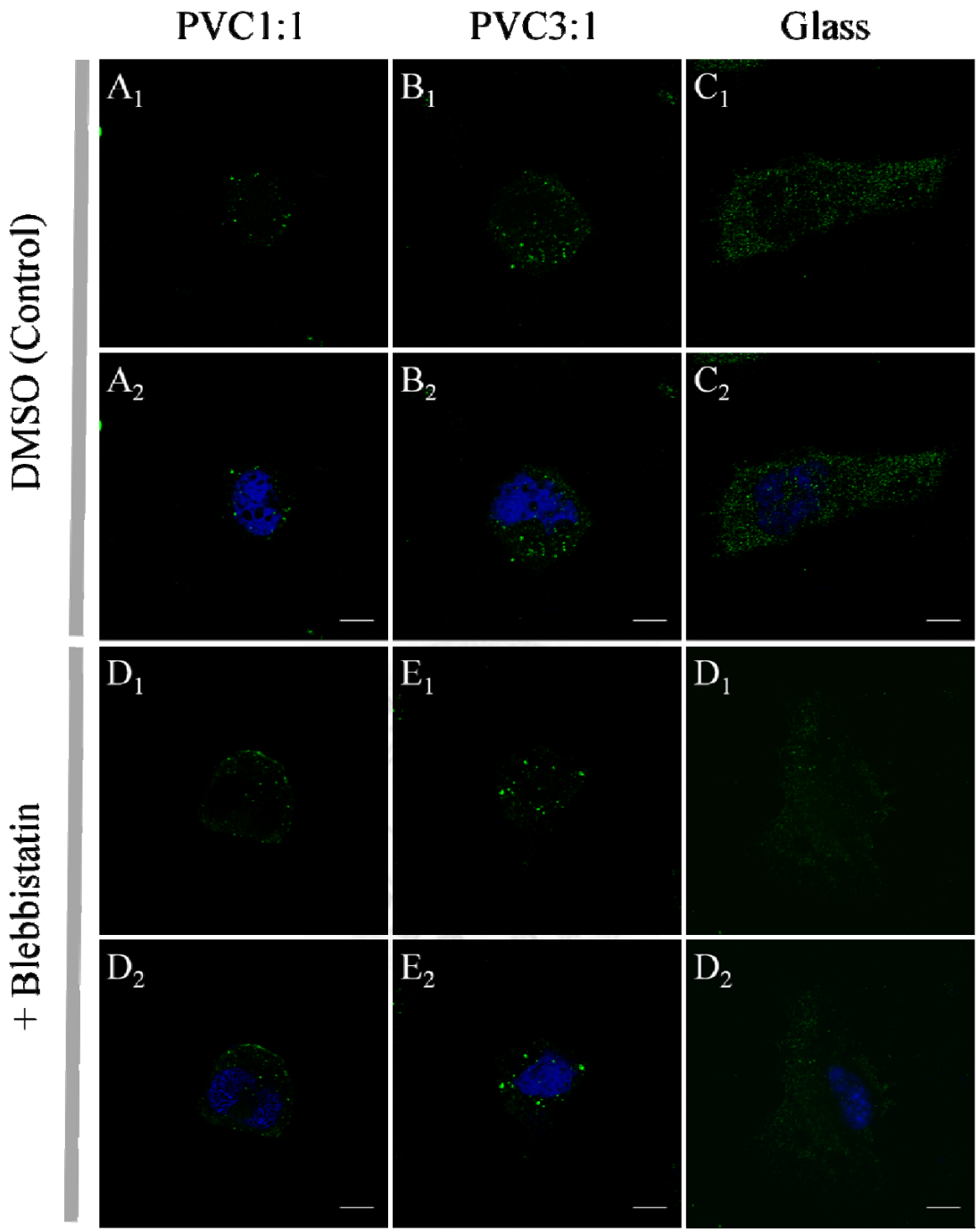

Figure 5-7. Focal adhesions of cells on different stiff with treatment of DMSO (control) or 30 μM Blebbistatin. Vinculin was stained to visualize the size of mature focal adhesions (Green). Nucleus was stained with DAPI (blue). (A-C) Cells cultured on PVC1:1 (A), PVC3:1 (B), and glass (C) were treated with DMSO as control. (D-E) Cells cultured on PVC1:1 (D), PVC3:1 (E), and glass (F) were treated with 30 μM Blebbistatin to inhibit myosin II-mediated contractility of stress fibers. (Scale bars = 10μm)

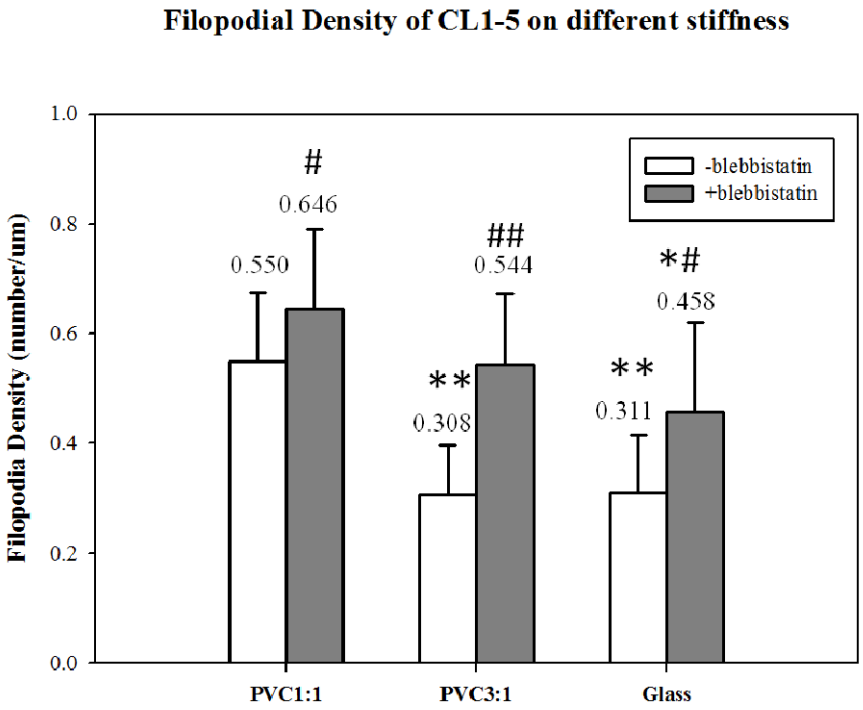

Figure 5-8. Treatment with blebbistatin increases the filopodial density on substrates with all stiffness. The white bars represent the cells without blebbistatin treatment, while the dark-gray bars represent the cells with blebbistatin treatment. Numbers above each bar represent the mean of filopodial density. Error bars indicate 95% confidence interval of the mean. Statistical cell number = 10, 13, and 10 for PVC1:1, PVC3:1, and Glass, respectively. * and ** represent the difference between different stiffness, $P < 0.05$ and $P < 0.01$, respectively. # and ## represent the difference between cells without and with blebbistatin treatment, $P < 0.05$ and $P < 0.01$, respectively.

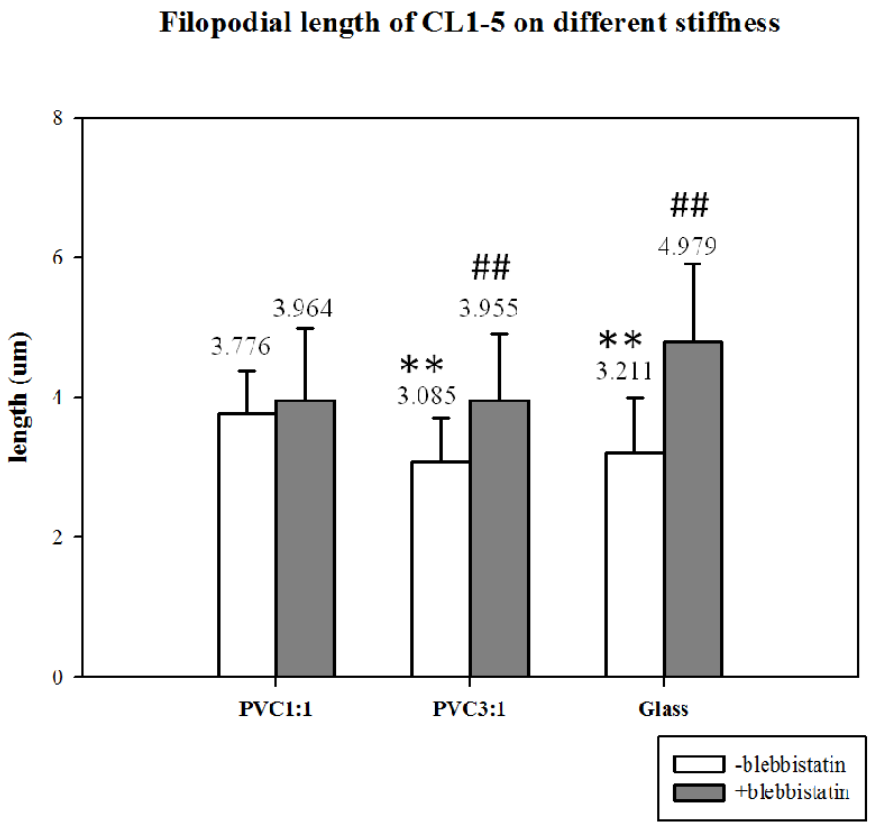

Figure 5-9. Treatment with blebbistatin increases the filopodial length on substrates with all stiffness. The white bars represent the cells without blebbistatin treatment, while the dark-gray bars represent the cells with blebbistatin treatment. Numbers above each bar represent the mean of filopodial length. Error bars indicate 95% confidence interval of the mean. Statistical cell number = 10, 13, and 10 for PVC1:1, PVC3:1, and Glass, respectively. * and ** represent the difference between different stiffness, $P < 0.05$ and $P < 0.01$, respectively. # and ## represent the difference between cells without and with blebbistatin treatment, $P < 0.05$ and $P < 0.01$, respectively.

Chapter 6 Discussion, Conclusion, and Future Work

6.1 Discussion

6.1.1 Increase in Filopodial Density and Length on Soft Substrates

Our study has uncovered an important mechanical role in the density and length of the filopodia, which are said to be correlated with the cell motility [1]. Culturing lung cancer cells on substrates with different stiffness at 20 kPa, 60kPa, and MPa, we saw more filopodial density and longer filopodial length on soft substrates than on stiff substrates. To study the underlying mechanism, we treated the cells with a myosin II inhibitor, blebbistatin, and found that the difference in filopodial density and length on different stiffness were compensated. This was consisted with the previous studies that the treatment with blebbistatin would cause an elongation in filopodial length and an increase in filopodial number and branching in neural cells [52-53]. Furthermore, inhibition of the myosin II by blebbistatin treatment inhibited the contractility of stress fibers, causing a decrease in maintenance and formation of stress fibers and focal adhesions [54]. Another study also reported that treating cells with blebbistatin could accelerate the cell migration [55]. This mimicked the situation of cells cultured on the soft substrates. Studies have reported that soft substrates inhibit Rho-induced formation

and α–actin assembly of stress fibers, disturb the maturation of focal adhesion, weaken the connection between the cytoskeletons and the focal adhesions, and further limit the contractility of the stress fibers, while the causal relationship of the above phenomena is still dubious and seems to be complementary [28-29, 56]. With the knowledge that the formations of stress fibers and filopodia are in antagonist pathways [28, 57], the increase in filopodial density and length of cell on soft substrates would result from the suppression of the stress fiber pathway.

In other respects, it should be considered that there is other mechanism to directly enhance the filopodia formation of cells on soft substrates. For example, it has been reported that mechanical strain in actin network increase the activity of FilGAP, which participates in Rho-pathway and down-suppresses the Rac activity [58]. Higher substrate stiffness would increase the contractility of stress fibers and the maturation of focal adhesions, and both could increase the strain in inside-out and outside-in mechanotransductions [59]. Another study also indicated that equibiaxial stretch decreased the activation of Rac [60]. As the results, stiff substrates might inhibit the Rac activity by increasing the strain of the cells. Although some studies have shown that the Rac activity was higher as cells adhered on substrates than as cells suspended, the active Rac involves in a number of distinct pathways, which lead to absolutely different cell responses [61-63]. Indeed, the total amounts of cellular Rac were equal in attached cells

and suspended cells; thus the competition between the formations of focal adhesions and filopodia should play a role [61]. Furthermore, the Rac activity defined in these papers was the bonding of Rac to PAK, which mainly involves in focal adhesion maturation, thus causing a result that fewer Rac proteins are available for filopodia formation as the cells are tightly adhered to the substrates. However, further measuring in the activity of Rac in filopodia forming pathway or other filopodial promoting proteins, such as Cdc42 and Arp2/3, is needed to clarify the mechanism of matrix-rigidity-modulating filopodial formation.

6.1.2 Correlation between Filopodial Stretching and Substrate Stiffness

Our study in filopodial stretching rate showed no correlation to the substrate stiffness. However, there have been numbers of research reporting that the focal adhesions on the filopodia could also sense the substrate stiffness. They showed that retraction rate is faster on stiff substrates, and the range is approximately from 0.05 μm/s to 0.6 μm/s, when adhesions occur or when there are no or weak adhesions respectively [26-27]. The protrusion rate might not be controlled by the substrate stiffness since the forming of focal adhesion is not yet completed, but the retraction rate might be. Therefore, our results of independence in filopodial retraction rate and its substrate stiffness could imply that the focal adhesions of filopodia might not yet form

and connect to the substrate. However, the retraction rates in our results were about 0.05μm/s - 0.07 μm/s, which seemed too slow if there were no adhesion or weak adhesions. As the results, this slow retraction rate might come from the time intervals of recording images we took. The time interval in our experiment was ten seconds. If a filopodia with retraction rate at 0.6 μm/s was tracked in two adjacent images, its starting length should be more than 6 μm and stretch in the same direction, or it would disappear on the next image or the rate would be underestimated. However, the mean and median of filopodial length was about 4μm, thus decreasing the chance of tracking a 6 μm-length filopodia. We also could not distinguish whether the filopodia changed their stretching directions within ten seconds. Therefore, we should shorten the time interval to trace those filopodia with higher stretching rate.

6.2 Conclusion

In our study, culturing cells on PVC substrate, which has high refractive index and tunable stiffness, could be applied in the SINAP system to study how cells respond to the mechanical stimuli. The Young's moduli of the resulting substrates ranged from 20 kPa to 60 kPa, which was compatible with the physiological range of tissue stiffness. We quantified the density and length of filopodia on different stiffness with the super-resolution SINAP images, and showed that the soft substrate would increase both

the density and length of filopodia, which implied an increase in cell motility. Further treatment with blebbistatin on stiff substrates could mimic the situation of the soft environments, thus explaining the role of stiff-enhanced focal adhesions and contractile stress fibers in cell response to environmental mechanical stimuli (fig. 6-1).

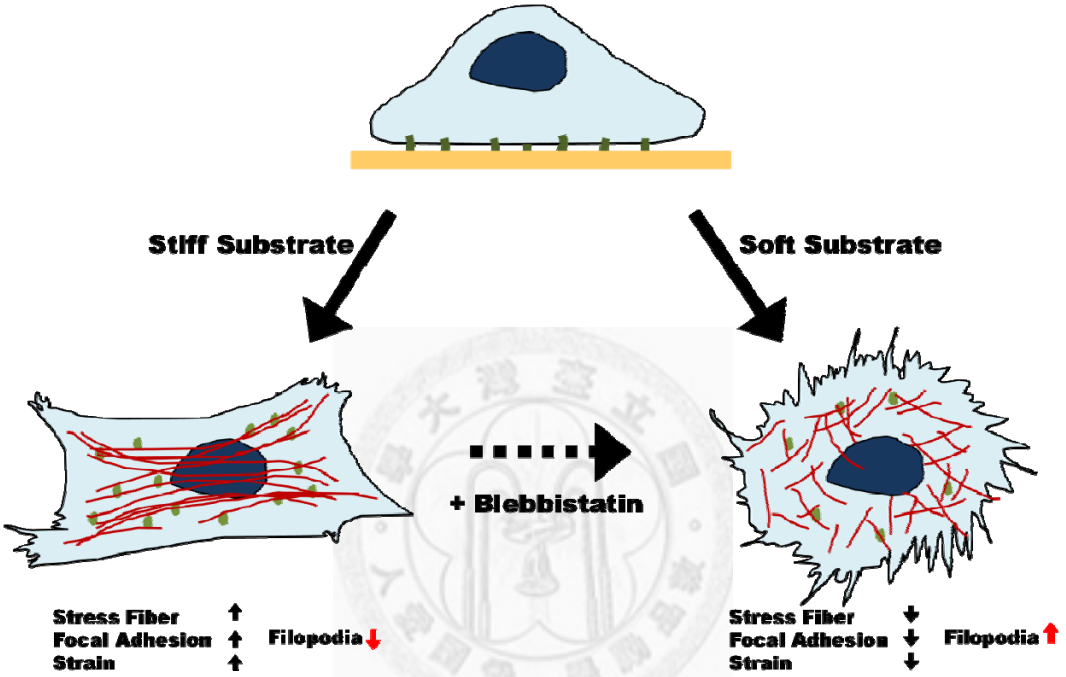

Figure 6-1. The model of the effects of substrate stiffness on filopodial formation. The cells on the stiff substrate show contractile stress fibers, static focal adhesions, and higher strain, thus inhibiting the filopodia formation. On the other hand, cells on the soft substrate show unorganized cytoskeletons, weak focal adhesions, and lower strain, thus promoting the filopodia formation. Treating cells with blebbistatin inhibits the contractility of the stress fiber and mimics the situation of the soft substrates.

6.3 Future Work

Our study connected the relation between substrate stiffness and filopodia formation. However, it has been reported that the spread area of cells are correlated with the substrate stiffness, and the spread area might also affect the formation of focal adhesions and stress fibers [5, 64]. To exclude the possibility that the soft substrates limit the formation of focal adhesions and stress fibers by decreasing the cell spread area, we should control the cell shape and spread area on different stiffness. Microcontact printing, which has been used in our lab, could be a chosen method to confine the cell spread area.

The active level of filopodia promoting proteins on different substrates should be the underlying mechanism of the rigidity-modulated filopodia formation as above-mentioned. Such as Rac, Cdc42, EGFR, and Arp2/3 are shown to participate in the filopodia formation. However, since the active levels of these proteins have not been connected to the mechanical stimuli, direct effects of the substrate stiffness on filopodia formations are still dubious.

The last, we speculated that the formation of filopodia was a feature of cell motility [1]. However, the previous studies were conducted on stiff cell-cultured dishes, and the morphology of cell motility is also cell-line specific [65]. Thus, we should still exam the motility of CL1-5 on different stiffness to confirm our model.

Reference

1. Machesky, L.M., *Lamellipodia and filopodia in metastasis and invasion.* Febs Letters, 2008. **582**(14): p. 2102-2111.
2. Gertler, F. and J. Condeelis, *Metastasis: tumor cells becoming MENAcing.* Trends in Cell Biology, 2011. **21**(2): p. 81-90.
3. Tzvetkova-Chevolleau, T., et al., *The motility of normal and cancer cells in response to the combined influence of the substrate rigidity and anisotropic microstructure.* Biomaterials, 2008. **29**(10): p. 1541-1551.
4. Guo, W.H., et al., *Substrate rigidity regulates the formation and maintenance of tissues.* Biophysical Journal, 2006. **90**(6): p. 2213-2220.
5. Discher, D.E., P. Janmey, and Y.L. Wang, *Tissue cells feel and respond to the stiffness of their substrate.* Science, 2005. **310**(5751): p. 1139-1143.
6. Guo, W. and Y. Wang, *The substrate rigidity regulates the formation and maintenance of tissues.* Molecular Biology of the Cell, 2004. **15**: p. 3A-3A.
7. Wang, Y.L., *Traction forces and rigidity sensing of adherent cells.* Conf Proc IEEE Eng Med Biol Soc, 2009. **2009**: p. 3339-40.
8. Buxboim, A., I.L. Ivanovska, and D.E. Discher, *Matrix elasticity, cytoskeletal forces and physics of the nucleus: how deeply do cells 'feel' outside and in?* J Cell Sci, 2010. **123**(Pt 3): p. 297-308.
9. Ridley, A.J., et al., *Cell migration: Integrating signals from front to back.* Science, 2003. **302**(5651): p. 1704-1709.
10. Jemal, A., et al., *Cancer Statistics, 2010.* Ca-a Cancer Journal for Clinicians, 2010. **60**(5): p. 277-300.
11. Geho, D.H., et al., *Physiological mechanisms of tumor-cell invasion and migration.* Physiology, 2005. **20**: p. 194-200.
12. Mattila, P.K. and P. Lappalainen, *Filopodia: molecular architecture and cellular functions.* Nature Reviews Molecular Cell Biology, 2008. **9**(6): p. 446-454.
13. Vacquier, V.D., *The connection of blastomeres of sea urchin embryos by filopodia.* Exp Cell Res, 1968. **52**(2): p. 571-81.
14. Faix, J. and K. Rottner, *The making of filopodia.* Current Opinion in Cell Biology, 2006. **18**(1): p. 18-25.
15. Knight, M.M., et al., *Live cell imaging using confocal microscopy induces intracellular calcium transients and cell death.* American Journal of Physiology-Cell Physiology, 2003. **284**(4): p. C1083-C1089.

16. Landry, S., et al., *Monitoring live cell viability: Comparative study of fluorescence, oblique incidence reflection and phase contrast microscopy imaging techniques.* Optics Express, 2004. **12**(23): p. 5754-5759.
17. Wang, C.C., et al., *Asymmetric cancer-cell filopodium growth induced by electric-fields in a microfluidic culture chip.* Lab on a Chip, 2011. **11**(4): p. 695-699.
18. Lee, C.H., H.Y. Mong, and W.C. Lin, *Noninterferometric wide-field optical profilometry with nanometer depth resolution.* Optics Letters, 2002. **27**(20): p. 1773-1775.
19. Lin, J.Y., et al., *Wide-field super-resolution optical sectioning microscopy using a single spatial light modulator.* Journal of Optics a-Pure and Applied Optics, 2009. **11**(1): p. -.
20. Lo, C.M., et al., *Cell movement is guided by the rigidity of the substrate.* Biophysical Journal, 2000. **79**(1): p. 144-152.
21. Georges, P.C. and P.A. Janmey, *Cell type-specific response to growth on soft materials.* Journal of Applied Physiology, 2005. **98**(4): p. 1547-1553.
22. Yu, H.M., J.K. Mouw, and V.M. Weaver, *Forcing form and function: biomechanical regulation of tumor evolution.* Trends in Cell Biology, 2011. **21**(1): p. 47-56.
23. Suresh, S., *Biomechanics and biophysics of cancer cells.* Acta Materialia, 2007. **55**(12): p. 3989-4014.
24. Kostic, A., C.D. Lynch, and M.P. Sheetz, *Differential Matrix Rigidity Response in Breast Cancer Cell Lines Correlates with the Tissue Tropism.* Plos One, 2009. **4**(7).
25. Paszek, M.J., et al., *Tensional homeostasis and the malignant phenotype.* Cancer Cell, 2005. **8**(3): p. 241-254.
26. Moore, S.W., P. Roca-Cusachs, and M.P. Sheetz, *Stretchy proteins on stretchy substrates: the important elements of integrin-mediated rigidity sensing.* Dev Cell, 2010. **19**(2): p. 194-206.
27. Chan, C.E. and D.J. Odde, *Traction Dynamics of Filopodia on Compliant Substrates.* Science, 2008. **322**(5908): p. 1687-1691.
28. Papakonstanti, E.A. and C. Stournaras, *Cell responses regulated by early reorganization of actin cytoskeleton.* Febs Letters, 2008. **582**(14): p. 2120-2127.
29. Park, J.S., et al., *The effect of matrix stiffness on the differentiation of mesenchymal stem cells in response to TGF-beta.* Biomaterials, 2011. **32**(16): p. 3921-3930.
30. 李超煌. *差動共焦顯微術及其應用*. 台灣大學電機工程研究所 博士論文 1997.

31. 王俊杰, *非干涉式廣視野光學測繪術及其應用*. 國立中正大學物理研究所博士論文, 2007.
32. 許慈軒, *以超解析率明視野光學顯微術觀測癌細胞絲狀偽足的動態變化*. 國立陽明大學光電工程研究所 碩士論文, 2007.
33. Neil, M.A.A., R. Juskaitis, and T. Wilson, *Method of obtaining optical sectioning by using structured light in a conventional microscope.* Optics Letters, 1997. **22**(24): p. 1905-1907.
34. 高于婪, *利用結構式照明奈米繪測術觀測癌細胞絲狀偽足在直流電場下的方向性生長*. 國立中正大學物理學研究所 碩士論文, 2010.
35. Cretu, A., P. Castagnino, and R. Assoian, *Studying the effects of matrix stiffness on cellular function using acrylamide-based hydrogels.* J Vis Exp, 2010(42).
36. Tse, J.R. and A.J. Engler, *Preparation of hydrogel substrates with tunable mechanical properties.* Curr Protoc Cell Biol, 2010. **Chapter 10**: p. Unit 10 16.
37. Kandow, C.E., et al., *Polyacrylamide hydrogels for cell mechanics: steps toward optimization and alternative uses.* Methods Cell Biol, 2007. **83**: p. 29-46.
38. Wang, C.C., K.L. Lee, and C.H. Lee, *Wide-field optical nanoprofilometry using structured illumination.* Optics Letters, 2009. **34**(22): p. 3538-3540.
39. Klee, D. and H. Hocker, *Polymers for biomedical applications: Improvement of the interface compatibility.* Biomedical Applications: Polymer Blends, 1999. **149**: p. 1-57.
40. Wilkes, C.E., et al., *PVC handbook*. 2005, Munich ; Cincinnati: Hanser. xxvi, 723 p.
41. Crespo, J.E., et al., *Substitution of di(2-ethylhexyl) phthalate by di(isononyl) cyclohexane-1,2-dicarboxylate as a plasticizer for industrial vinyl plastisol formulations.* Journal of Applied Polymer Science, 2007. **104**(2): p. 1215-1220.
42. Wadey, B.L., *An innovative plasticizer for sensitive applications.* Journal of Vinyl & Additive Technology, 2003. **9**(4): p. 172-176.
43. RodriguezFernandez, O.S. and M. Gilbert, *Aminosilane grafting of plasticized poly(vinyl chloride) .2. Grafting and crosslinking reactions.* Journal of Applied Polymer Science, 1997. **66**(11): p. 2121-2128.
44. Storck, J., H. AbDelRazek, and E.R. Zimmermann, *Effect of polyvinyl chloride plastic on the growth and physiology of human umbilical vein endothelial cells.* Biomaterials, 1996. **17**(18): p. 1791-1794.
45. Buckley, M.R., et al., *Mapping the depth dependence of shear properties in articular cartilage.* Journal of Biomechanics, 2008. **41**(11): p. 2430-2437.
46. INSTRON, *Instron 8848 MicroTester Reference Manual.*
47. Choi, W., et al., *Tomographic phase microscopy.* Nature Methods, 2007. **4**(9): p. 717-719.

48. Wong, J.Y., et al., *Directed movement of vascular smooth muscle cells on gradient-compliant hydrogels.* Langmuir, 2003. **19**(5): p. 1908-1913.
49. Engler, A.J., et al., *Matrix elasticity directs stem cell lineage specification.* Cell, 2006. **126**(4): p. 677-689.
50. Jung, C.H., et al., *Patterning of cells on a PVC film surface functionalized by ion irradiation.* Polymers for Advanced Technologies, 2010. **21**(2): p. 135-138.
51. Ahmed, S., et al., *Poly(vinylmethylsiloxane) Elastomer Networks as Functional Materials for Cell Adhesion and Migration Studies.* Biomacromolecules, 2011. **12**(4): p. 1265-1271.
52. Gehler, S., et al., *Brain-derived neurotrophic factor regulation of retinal growth cone filopodial dynamics is mediated through actin depolymerizing factor/cofilin.* Journal of Neuroscience, 2004. **24**(47): p. 10741-10749.
53. Medeiros, N.A., D.T. Burnette, and P. Forscher, *Myosin II functions in actin-bundle turnover in neuronal growth cones.* Nature Cell Biology, 2006. **8**(3): p. 215-226.
54. Hotulainen, P. and P. Lappalainen, *Stress fibers are generated by two distinct actin assembly mechanisms in motile cells.* Journal of Cell Biology, 2006. **173**(3): p. 383-394.
55. Liu, Z.A., et al., *Blebbistatin inhibits contraction and accelerates migration in mouse hepatic stellate cells.* British Journal of Pharmacology, 2010. **159**(2): p. 304-315.
56. Pasapera, A.M., et al., *Myosin II activity regulates vinculin recruitment to focal adhesions through FAK-mediated paxillin phosphorylation.* Journal of Cell Biology, 2010. **188**(6): p. 877-890.
57. Burridge, K. and R. Doughman, *Front and back by Rho and Rac.* Nature Cell Biology, 2006. **8**(8): p. 781-782.
58. Ehrlicher, A.J., et al., *Mechanical strain in actin networks regulates FilGAP and integrin binding to filamin A.* Nature, 2011. **478**(7368): p. 260-U154.
59. Provenzano, P.P. and P.J. Keely, *Mechanical signaling through the cytoskeleton regulates cell proliferation by coordinated focal adhesion and Rho GTPase signaling.* Journal of Cell Science, 2011. **124**(8): p. 1195-1205.
60. Katsumi, A., et al., *Effects of cell tension on the small GTPase Rac.* Journal of Cell Biology, 2002. **158**(1): p. 153-164.
61. del Pozo, M.A., et al., *Adhesion to the extracellular matrix regulates the coupling of the small GTPase Rac to its effector PAK.* Embo Journal, 2000. **19**(9): p. 2008-2014.
62. Gallegos, L., M.R. Ng, and J.S. Brugge, *The myosin-II-responsive focal adhesion proteome: a tour de force?* Nature Cell Biology, 2011. **13**(4): p. 344-+.

63. Kuo, J.C., et al., *Analysis of the myosin-II-responsive focal adhesion proteome reveals a role for beta-Pix in negative regulation of focal adhesion maturation.* Nature Cell Biology, 2011. **13**(4): p. 383-U109.
64. Chen, C.S., et al., *Geometric control of cell life and death.* Science, 1997. **276**(5317): p. 1425-1428.
65. Friedl, P. and S. Alexander, *Cancer Invasion and the Microenvironment: Plasticity and Reciprocity.* Cell, 2011. **147**(5): p. 992-1009.